Synthesis and Electrochemical Performance of $SnO_x/Ti_3C_2T_x$ Anodes for Li-ion Batteries

by

Hengze Chen

A thesis submitted to the Graduate Faculty of
Auburn University
in partial fulfillment of the
requirements for the Degree of
Master of Science

Auburn, Alabama
May 04, 2019

Keywords: MXene, Energy storage, Tin Oxide Anode, Lithium Battery

Approved by

Majid Beidaghi, Chair, Assistant Professor of Material Engineering Dong-Joo Kim,
Professor of Materials Engineering
Xiaoyuan Lou, Associate Professor of Materials Engineering

Abstract

Modern society has a higher requirement and need for high-capacity and stable energy storage and conversion devices. 2D materials are a group of emerging materials that have shown advantages in energy, catalysis, and mechanical applications. This research focuses on introducing a microwave-assisted method to synthesize hybrid structures and improve the electrochemical performance of layered $Ti_3C_2T_x$, which has been recently introduced as an anode material for lithium-ion batteries. In this study, hybrid structures of $SnO_x/Ti_3C_2T_x$ are synthesized and the effects of microwave synthesis parameters on the electrochemical performance of the synthesized hybrid electrodes are investigated. Through several materials and structural characterization methods, it is shown that the SnO_x deposited $Ti_3C_2T_x$ material maintained its layered structure and the hybrid material has a stable cyclic performance when tested as an anode for lithium-ion batteries. Our studies show that if microwave parameters are tailored and carefully controlled, oxidation of MXene during synthesis can be avoided. Further, as a mechanically robust 2D material, the MXene flakes can support the volume change of tin oxide upon electrochemical reaction with Li and therefore significantly improve the cyclability of the hybrid structure.

Acknowledgment

I am very grateful for the support and help I have received over the course of my research from my advisor, Dr. Beidaghi. I want to thank my group members Emre Kayali and Jafar Orangi. Further, I am thankful for Armin VahidMohammadi for his help with performing the SEM and XRD analyses as well as his guidance in performing the electrochemical tests which helped me a lot to finish this project. I also appreciate the help from Dr. Sanghamitra Deb from Alabama University or performing the TEM characterizations.

Table of Contents

List of Figure

List of Table

Chapter 1: Introduction

1.1 Overview

Today, the social developments, the change in our lifestyles, and an increasing population bring huge demand for energy resources. The energy consumption of the world would be at least 10^{10} tons of oil per year after 2050, as shown in **Fig. 1.1**.[1] Traditional fossil fuels have high energy density and are easily accessible which make them the most important energy resource we rely on. However, fossil fuels have limited reserves in nature, and their production will be harder to meet our future energy requirements. Another problem is the high carbon emission during the energy transformation process when burning fossil fuels. The concentration of CO_2 in the atmosphere has already risen to more than 400 ppm, which is 148.8% higher than what it was at the beginning of the industrial revolution. The rise in CO_2 emission is one of the main causes of global warming. Gases such as NO_x or SO_x are side products of burning fossil fuels and a main source of air pollution.[2] These problems are the driving motivation for researchers to find out possible methods to overcome the limitations of

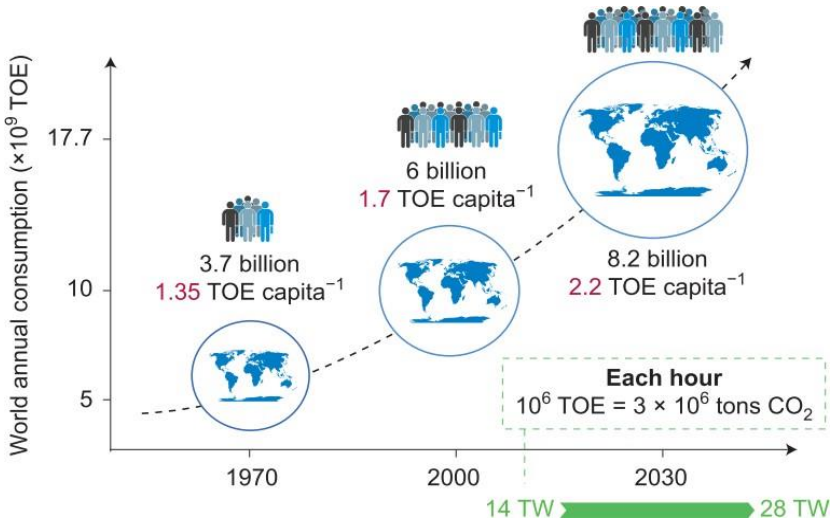

Fig.1.1 The global population and energy requirement yearly in 1970, 2000 and 2030, TOE= ton of oil equivalent.[1]

traditional energy resources.

To alleviate the conflict between the increasing demand for energy resources and consumption of fossil fuels, one important research topic is finding renewable and environmentally friendly energy resources and accompanying storage devices. Great efforts have been put on increasing energy collection and conversion efficiency of renewable energy sources such as solar and wind energy. However, compared with fossil fuels, new types of energies are widely dispersed and intermittent so that their energy density and conversion efficiency is much lower. For example, the geographical distribution of a solar power station and daylight availability are limiting factors for solar power's application. In order to solve this problem, high-performance energy storage devices like batteries and supercapacitors with favorable electrochemical (long cycling stability and high capacity) and mechanical properties are necessary.[2–4]

1.2 Lithium-ion battery

Batteries are essentially electric energy storage devices with one or more electrochemical cells. In the past 150 years, with the development of technology in battery performance and related areas, batteries find their place in daily human life. Among different battery technologies, lithium-ion batteries (LIBs) are extensively practical in modern society since it has good cyclability, high capacity, and acceptable safety. Basically, LIBs transform chemical energy to electric energy. Today, the commercial lithium-ion battery usually uses graphite as the anode material and $LiCoO_2$ as its cathode material, (Fig. 1.2).[5]

Batteries are components that affect the reliance of hybrid vehicles on fossil fuels and working hours of mobile smart devices. Therefore, their specific capacity needs to be increased to satisfy future needs. A reasonable research direction for enhancing LIBs is finding better replacement electrode materials since the charge storage properties of the device mainly depend on the electrochemical properties of the electrode materials. Graphite as an anode material in LIB system has advantages including high stability, safety, and low cost. On the other hand, the theoretical capacity of graphite is only 372 mAh g^{-1} which restricts a battery's electrochemical performance (specific power density and specific energy density). Comparing graphite with other potential electrode materials, such as transition metal oxides (like SnO_x and CoO_4), Si, and even lithium metal itself shows that graphite has lower theoretical specific capacity. Since the

theoretical specific capacity of the anode material graphite cannot meet today's expectations, finding a better replacement for graphite can help engineers design an improved energy storage device. To make those materials work efficiently in commercial LIB system, researchers have aimed to overcome structural and technical problems presented by electrode materials such as solid/electrolyte-interphase (SEI) formation, volume expansion in the charge/discharge process, and chemical and structure deterioration of the electrode materials.[6–10] In **Fig. 1.3**,[11] the schematic of the working mechanism of a commercially availsable LIB is presented.

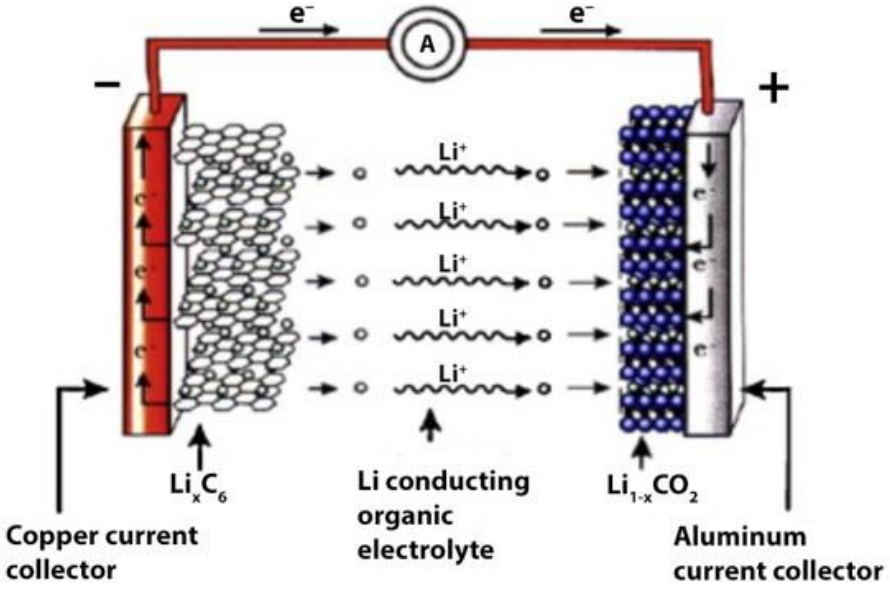

Fig.1.2 Schematic of a commercially available LIB's working mechanism.[5]

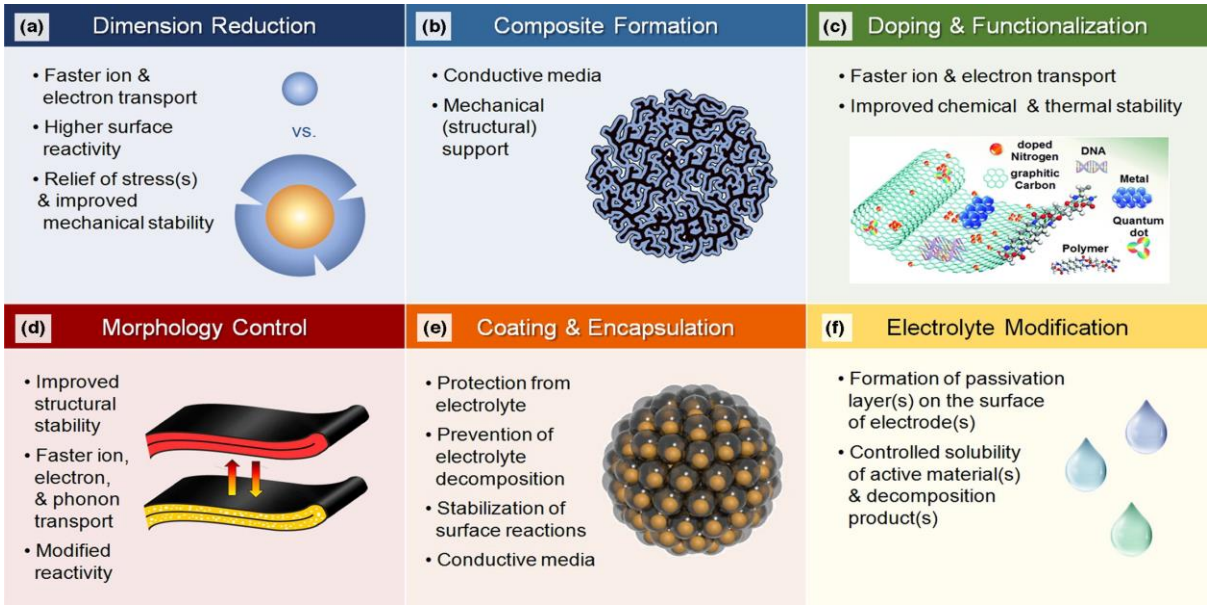

Fig.1.3 General methods to improve LIBs performance, include: (a) reducing dimensions of active materials, (b) formation of composites, (c) doping and functionalizing, (d) tuning particle morphology, (e) formation of coatings or shells around active materials, and (f) modification of electrolyte. [11]

1.3 Supercapacitor

The other important electrochemical energy storage device, supercapacitors, work with different mechanisms like electric double layer capacitance (EDLC) or pseudocapacitance. Supercapacitors are promising devices as a replacement for batteries in the energy storage field mainly due to long-life cycle, high-power density, and fast charge/discharge rate. In principle, EDLC collects and releases electric charges through the positive and negative ion adsorption on the electrode material surface with different electronic properties. The charge storage EDLC devices are originated from a simple physical process, and therefore these devices have a fast rate of charge and discharge. Carbon-based materials with large specific surface area, like carbon nanotubes (CNTs) and graphene are considered as good candidates for EDLC electrodes.[6,12]

The working principle of pseudocapacitors is based on the fast and reversible faradic redox reaction which occurs at the electrode surface or near the surface. Because of various

oxidation states of the electrode materials used in these devices, the charge transfer between electrolyte and electrode material can provide higher energy density than EDLC. In the same working area of an electrode whose's performance is dominated by the pseudocapacitance mechanism, the capacitance can be 10 to 100 times more than an EDLC with a similar working area.[13] Even though there are many advantages for supercapacitors, their commercial application is limited by their relatively low energy density, which is about 5-10 Wh/Kg which is lower than lead-acid batteries.[14] Due to the limitations and problems hindering the electrochemical performance of supercapacitors, their commercialization faces some obstacles. In order to use supercapacitors commercially, researchers have to overcome the issues and improve their performance.

1.4 Applied material introduction

1.4.1 Background and synthesis method of MXene

As **Fig.1.3b** shows, the formation of a composite material synthesized from various electroactive materials is one of the most important methods to improve the electrochemical performance of electrode materials. Recent research shows the improved performance of composite electrode materials, or hybrid electrode materials, due to the synergistic effects of various components on the electrochemical performance of the electrodes. Two-dimension (2D) materials are reported to show promising performance due to their structural and morphological advantages compared with particle systems when used as electrode material in LIBs. Graphene, for example, as an emerging 2D material is a good candidate to work as supercapacitor electrode material. It has attracted research interest as it has a good theoretical capacity value up to 550 F g^{-1} as an EDLC. This value can even reach to 739 F g^{-1} after further modifications (for instance, nitrogen doping treatment).[6,12] Three-dimensional (3D) graphene framework with or without a hierarchical porous structure has been reported as an electrode material for LIBs with improved specific capacity, which was about 472 mAh g^{-1} at 5 A g^{-1} current density.[15–17] From these reports, the carbon-based or carbide materials are considered as an important type of materials which can play a significant role in the future of electrode material for energy storage with superior electrochemical and structural properties.

In this study, a novel layered material, MXene, is introduced as the conductive support

for the deposition of tin oxide nanoparticles and the synthesized hybrid electrode materials are used as an efficient anode material in LIB system. Tin oxide is a promising anode material for LIB, however unstable structure and extensive volume change during cycling limits its application. Synthesizing a hybrid material with 2D MXene as support for tin oxide can be one of the possible solutions to improve tin oxide's electrochemical performance. Since MXene was first discovered in 2011, they have exhibited many interesting physical, chemical, and electrochemical properties and have inspired research to explore their potential applications in different scientific fields.[18]

MXenes are a group of layered transition metal carbides, carbonitrides and nitrides with general formula $M_{n+1}X_nT_x$ (n=1,2,3). The M is early transition metal (Ti, V, Zr, Ta, Nb, etc); X is carbon and/or nitrogen, and T represents the surface termination groups (-OH, -O, and -F). MXenes are synthesized by selective etching of metal from the structure of MAX phases, which are a large family of ternary layered carbides. Unlike graphite and many other layered materials that conserve their layered structure with weak Van der Walls forces between the layers, the chemical bond in MAX phase is the combination of ionic and metallic bonds which makes it hard to separate the layers by physical methods. Therefore, to produce layered MXenes from MAX phases, acids such as hydrofluoric acid (HF) are used to selectively remove the A layer from the corresponding MAX phase (usually Al or Si), since the bond strength between M-A (metallic bond) is weaker than M-X (ionic bond). **Fig. 1.4** showed the required steps to synthesize 2D MXene flakes from the MAX phase using HF followed by an exfoliation step.[19,20] Etching and sonicating results in a stable colloidal solution of 2D MXene flakes. Further treatment can be applied to improve the solution properties.

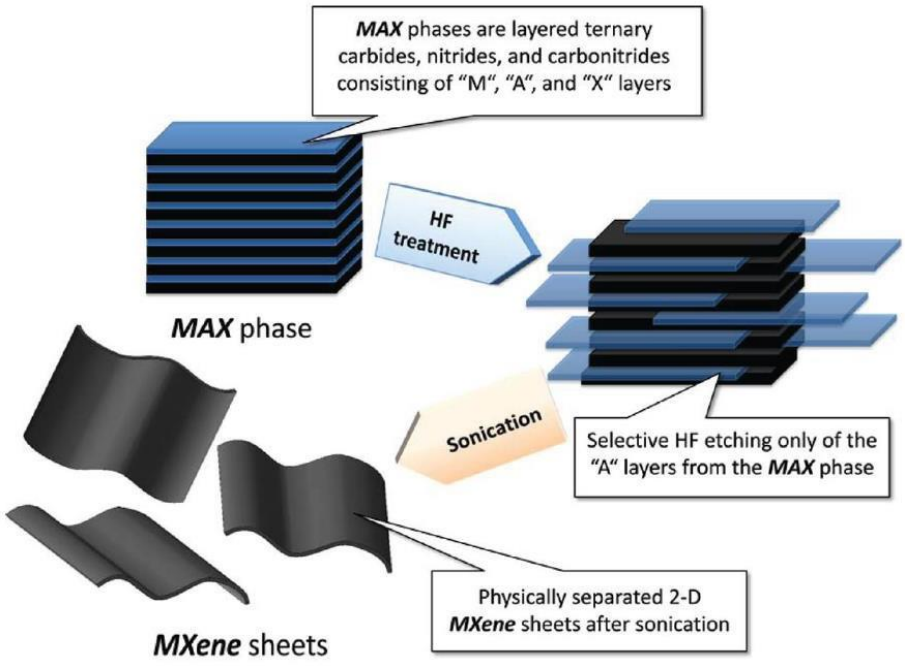

Fig.1.4 Schematic of MXene sheets synthesis process.[19]

Recent studies and the modification of the etching process resulted in hydrochloride acid (HCl) and lithium fluoride (LiF) solution as the etchant. This acid-salt solution helps to reduce the use of hazardous HF and makes the process safer.[18,21] The surface termination groups on the MXene surface usually come from the etching process and affect the electrochemical and electrical properties of MXenes and their structural stability. For example, density functional theory (DFT) calculations have shown that O-terminated MXene has higher capacity in LIBs. [18,22] The termination groups can also be the reason for the instability of MXenes in some environments, causing MXene oxidation.[19,23,24]

In the proposed experiment, the applied etching method is a mild etching method which used LiF and HCl mixture to replace HF(**Fig. 1.5)**.[25] The etching process removes layers of Al atoms from Ti_3AlC_2 structure. The Li-ions intercalate into the etched powder and increase the interlayer spacing between adjacent layers. Following that, the MXene can be delaminated with further processing (sonication) to achieve 2D $Ti_3C_2T_x$ flakes dispersed in water. Changing the surface termination groups through chemical modification is a possible way to achieve a MXene

with favorable properties, since those groups provide rich reaction sites.

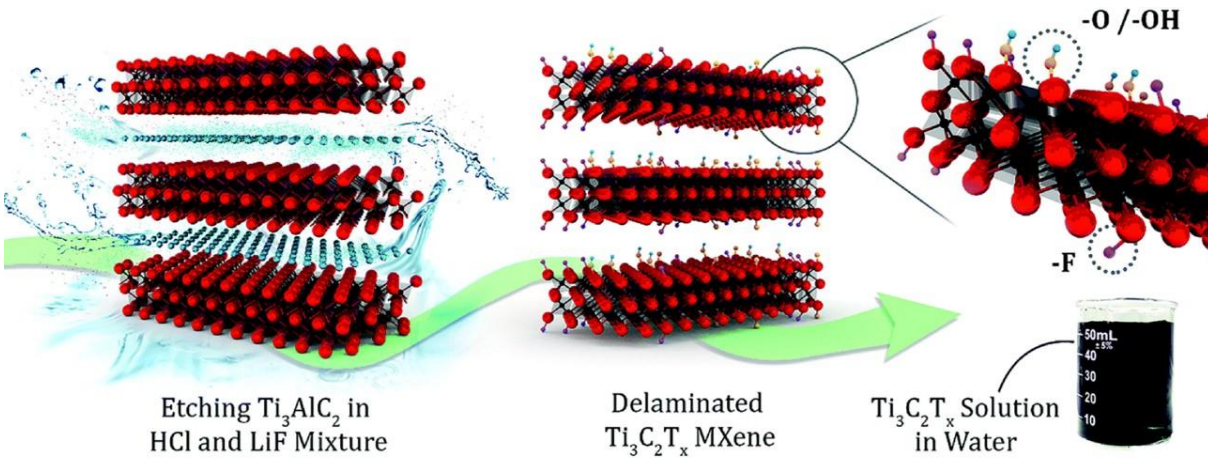

Fig.1.5 Schematic of the etching process for preparing $Ti_3C_2T_x$ colloidal solution.[25] Al atoms are removed, and Li ions intercalate between the layers.

1.4.2 Energy storage application of MXene

So far, more than 25 different MXenes has been reported, including $Ti_3C_2T_x$, V_2CT_x, Nb_2CT_x which have demonstrated promising performances in energy storage related fields. Among them, $Ti_3C_2T_x$ has attracted more attention because of its outstanding electrochemical properties such as high electrical conductivity, hydrophilicity, and low lithium diffusion barrier (0.07 eV), which is even lower than graphite (0.3 eV). [3,4] These interesting properties render $Ti_3C_2T_x$ MXene as a potential candidate for the anode of LIBs with high capacity and high rate capability. Other characteristics of $Ti_3C_2T_x$ which distinguish it from other emerging lithium battery anode materials include its low insertion voltage for Li^+ (0.2 to 0.6 V vs. Li/Li^+) and ability to perform at high rates and for a long number of cycles.[20] Density functional theory (DFT) calculations have suggested a theoretical capacity of $Ti_3C_2T_x$ in LIB system is about 320 mAh g^{-1}. In addition, $Ti_3C_2T_x$ MXene's electrochemical properties can be improved significantly by hybridizing it with other organic/inorganic materials with high capacities or modification in its surface terminal group.[20,26,27]

In different energy storage devices, MXenes have already shown promising properties. The polyaniline/$Ti_3C_2T_x$ supercapacitor electrode has a gravimetric capacitance of up to 503F g^{-1} and volumetric capacitances of 1682 F cm^{-3}. [25]Furthermore, after 10,000 cycles, it could maintain 98.3% of its initial capacitance. In the case of Li-S batteries, alkalized $Ti_3C_2T_x$ nanoribbon-based electrode structures with polypropylene (PP) separator showed the capacity of 1062 mAh g^{-1} at 0.2 C and 632 mAh g^{-1} at 0.5 C, while delivering 288 mAh g^{-1} at an extremely high rate of 10 A g^{-1}. It was suggested that the MXene film could work well on PP separator and enhance ionic diffusion.[28] Beyond lithium-ion battery devices, MXenes have also shown promising performances. For example, when V_2CT_x was used as the aluminum ion battery cathode, capacities above 300 mAh g^{-1} were achieved at a current density of 100 mA g^{-1}.[29] Also, our group has also shown cation pillared structures fabricated from delaminated V_2CT_x with superior (electro)chemical stability that could perform as freestanding binder-free electrode materials for aqueous supercapacitors, delivering volumetric capacitances in excess of 1300 F cm^{-3} and a capacitance retention of ~77% after one million cycles.[30]

1.4.3 Transition metal oxides for energy storage applications

Transition metal oxides (TMOs) are a group of important electrode materials with high specific capacities, which have attracted considerable attention as LIB electrode materials. During battery cycling, it is suggested that the crystal structures of TMOs undergo a slight change due to the topotactic reactions that occur.[31]

A high-performance electrode material should meet the following requirements. First, it should be able to host the intercalating cations, where a 2D structure or a 3D lattice structure capable of lithium-ion intercalation and deintercalation is desired. TMOs' crystal structure gives them such properties for Li^+ intercalation. In today's commercial lithium batteries, the cathode is usually made up of Li-rich TMOs like $LiCoO_2$ or $LiFePO_4$ since their structure, and achievable capacity can meet the required demand for different applications.[32] TMOs have also shown promising performances as anode materials for LIBs where usually they are combined with other conductive materials to form composites or hybrid structures .[33]

As indicated, MXenes can be considered as promising electrode materials for LIBs. In this study, we have fabricated a hybrid $SnO_x/Ti_3C_2T_x$ material through microwave-assisted hydrothermal synthesis method and investigated its electrochemical performance as a lithium

battery anode material. The synthesis method, characterization process and electrochemical performance of $SnO_x/Ti_3C_2T_x$ hybrid material will be discussed in detail in the following chapters. The experimental results confirmed that this hybrid material, which can be synthesized in a few minutes, can deliver a high specific capacity as well as excellent cyclic stability, rendering it as a potential anode material for future LIBs.

Chapter 2: Microwave assisted $SnO_x/Ti_3C_2T_x$ lithium battery anode

2.1. Introduction

TMOs have shown promise as high capacity LIB electrode materials.[32] When TMOs are tested as LIBs' anode, they can deliver higher capacities than the conventional commercial anode, graphite, since they are capable of storing more than 6 Li^+ per unit formula during battery charging-discharging. TMOs such as Co_3O_4, Fe_3O_4, MnO_2 and SnO_2, are among the structures with high theoretical specific capacities.[8,10,34,35] Their specific capacity can reach values higher than 750 mAh g^{-1}, and since their operating voltage windows are wide enough, they are usually considered as promising anode materials .[36–38] However, the large expansion and volume change of TMO nanomaterials during lithium intercalation/de-intercalation leads to their mechanical breakage and crystal structural degradation, which results in fast capacity decay after the first few cycles. Therefore, combining TMOs on structures that support such volume change can be a useful strategy to inhibit this problem. Since MXenes have good conductivity as well as mechanical robustness, fabrication of the hybrid material, TMO/MXene, should result in a structure that could potentially solve these issues and deliver long-life and high specific capacities in the LIB system.

The transition metal oxide used in this project is SnO_2, which has a high theoretical capacity of 1494 mAh g^{-1} indicating about four times higher lithium storage capability compared to graphite anode.[39] It has a low insertion voltage range of 0.005 to 1.0 V (Voltage Vs. Li^+/Li). However, a large volume change (more than 300%) occurs when SnO_2 is inserted with Li ions, which limits its application as a practical electrode. Besides, tin metal aggregation phenomenon happens when it works in LIBs, this is another structural problem that needs to be addressed.[31]Also, the thick SEI layer formation in electrodes based on this material makes capacity fade drastically in the first few cycles.[40] Also, the other intrinsic properties of TMOs such as low electrical conductivity result in a poor high-rate capability for SnO_2 .[31] Therefore,

hybridizing SnO_2 in a structure that can address some of these shortcomings seems to be a reasonable method to achieve better performing anode materials through combining advantages from both materials in the hybrid structure.

Earlier reports have shown promising results for hybrid electrodes of TMO and 2D materials. 2D materials provide a highly conductive support network that significantly improves the charge transport properties of the electrode and its rate-capability.[4,16] In addition, the flexible nature and excellent mechanical properties of 2D materials can enhance the mechanical robustness of the hybrid electrode materials and accommodate the large volume change of TMOs during battery cycling, improving their cycle life, and minimizing the electrode structure degradation.[6] In some earlier cases, TMOs deposited on graphene oxide (GO), or reduced graphene oxide (rGO) showed remarkable stability and capacity.[31] The sandwich structures of graphene–MnO_2 –GNRs, as a LIB anode has a capacity up to 890 mAh g^{-1} at 100 mA g^{-1}, and the graphene layers accommodate the volume change during charge/discharge and reduce the TMOs structural loss.[36] The SnO_2 deposited single-wall carbon nanotubes on graphene (SnO_2@G-SWCNT) aerogels have a capacity of 785 mAh g^{-1} at 100 mA g^{-1} after 200 cycles.[41] In terms of MXenes, an important property of $Ti_3C_2T_x$ is the interlayer distance which will increase upon cycling since the Van der Wall's force between layers is weak and the lattice can expand when some organic molecules or ions are inserted between them. This can lead to improved electrochemical performance when MXenes are used as the anode material for LIBs.[4]

Inspired by the early works in this field, we deposited SnO_x on $Ti_3C_2T_x$ through the microwave-assisted synthesis method and were able to synthesize a high specific capacity anode material. The synthesized hybrid materials could deliver a reversible capacity of 430.4 mAh g^{-1} after 600 cycles at 2 A $g^{-1}$with a high Coulombic efficiency. In a similar microwave reaction condition, other types of TMOs were deposited on $Ti_3C_2T_x$ flakes, to demonstrate the generality of our approach for fabrication of high-performance TMO/MXene anode materials.

2.2 Experimental section

Preparation of Ti_3AlC_2 MAX phase: The Ti_3AlC_2 MAX phase was synthesized as follow. First, TiC, Ti and Al powders (99.5%, Aesar) were mixed in 0.85:1.15:1.05 ratio in a container and ball milled for 24h. After heating it at 1400℃ (5℃/min) for 4h, a Ti_2AlC block

was obtained. Then the block was milled and sieved. The Ti_2AlC powder was mixed with TiC, using zirconia grinding ball milling for 24h again with a Ti_2AlC: TiC ratio of 1:1. The brick was heated to 1400 ℃ after 2h (5℃/min) to get Ti_3AlC_2 brick. The Ti_3AlC_2 powder is ready after milling and sieving.[42]

Synthesis and Delamination of $Ti_3C_2T_x$: After adding 2 g of LiF into 40 ml 6 M HCl and mix them together, 2g Ti_3AlC_2 was added into the solution in an ice bath. After transferring the container into a 35°C water-bath, the solution was stirred for 24h. Afterward, the etched power was washed several times using DI water and by centrifuging the suspension at 3500 rpm for 5 minutes each time until the supernatant pH was close to 6. Then the powders were added to 150 mL water and were probe sonicated for 1h to obtain the delaminated $Ti_3C_2T_x$. The obtained solutions were then argon bubbled for 1h to remove any dissolved oxygen and they were stored in the refrigerator.[42]

Microwave-assisted deposition of TMOs on MXene nanosheets. TMO deposited $Ti_3C_2T_x$ nanosheets were synthesized by microwave assisted hydrothermal reaction as shown in **Fig.2.1a**. In short, SnO_x/ $Ti_3C_2T_x$ was prepared as follows. After measuring the concentration of the $Ti_3C_2T_x$ supernatant, different weight ratios of $SnCl_2$ to MXene (1:10, 1:1 and 10:1) were prepared by dissolving the required amount of $SnCl_2$ in 1-3 ml DI water. Then, about 60ml of ethylene glycol (EG) was added to 20ml of $Ti_3C_2T_x$ supernatant (volume ratio of EG: water is 3:1), and they were mixed for a few minutes. 20 ml of the mixed solution was then transferred to a microwave reactor container. All reactions were performed at 180°C at 850 W power. The reaction times were varied to find the optimum time, which is changing from 5 min, 10 min, 15 min, and 20 min. At this step, the powders in the colloidal suspension were collected by centrifuging the solution at 3500 rpm for 5 min. The precipitate was washed twice with DI water to remove extra EG. The powder solution was filtered, collected, and was dried under vacuum at 50°C overnight.

To synthesize the $MnO_2/Ti_3C_2T_x$, $MnCl_2.4H_2O$ was used as Mn^{2+} source, a 10:1 $MnCl_2/Ti_3C_2T_x$ weight ratio was prepared. $MnCl_2.4H_2O$ was dissolved in 1-3 ml DI water. The remaining part of the process was similar to that of $SnO_x/Ti_3C_2T_x$.

To prepare $MoO_3/Ti_3C_2T_x$, 200 mg $MoCl_3$ was dissolved in a mixed solution consisting

of 15 ml DI water, 5 ml ethanol and 0.25 ml nitric acid to make 9.87 mg/ml $MoCl_3$ solution.[37] A few drops of this solution were added to $Ti_3C_2T_x$ solution to make a 1:1 weight ratio of $MoCl_3$: $Ti_3C_2T_x$. The solution was transferred to a microwave container and processed according to the procedure mentioned above.

2.3 Structural characterizations and electrochemical measurements.

The battery anode material was prepared through a slurry casting method. After mixing and stirring SnO_x/ $Ti_3C_2T_x$ powder with carboxymethylcellulose sodium salt (CMC) and carbon black in an 8:1:1 ratio (DI water was used as the solvent) overnight, the slurry was cast on copper foil and dried under vacuum oven at 80 ℃. The electrolyte (1M $LiPF_6$ in 1:1 EC: DEC) was prepared by mixing ethylene carbonate (EC) and diethyl carbonate (DEC) in a 1:1 volume ratio and the 1M equivalent of $LiPF_6$ salt were dissolved in the mixture at room temperature. After casting, the mass loading of the dry slurry was about 0.42 to 2.5 mg cm^{-2} on each punched copper foil surface, which were directly used to assemble the coin cells. The casted anode and the other components used to assemble the coin cells are shown in **Fig .2.2**. The anode was prepared by punching a 7 mm diameter circular sample. CR-2032 coin cells were used to prepare half-cells in the argon-full glovebox with water and oxygen level of lower than 0.1 ppm. All the specific capacity calculations were based on the mass of the active material.

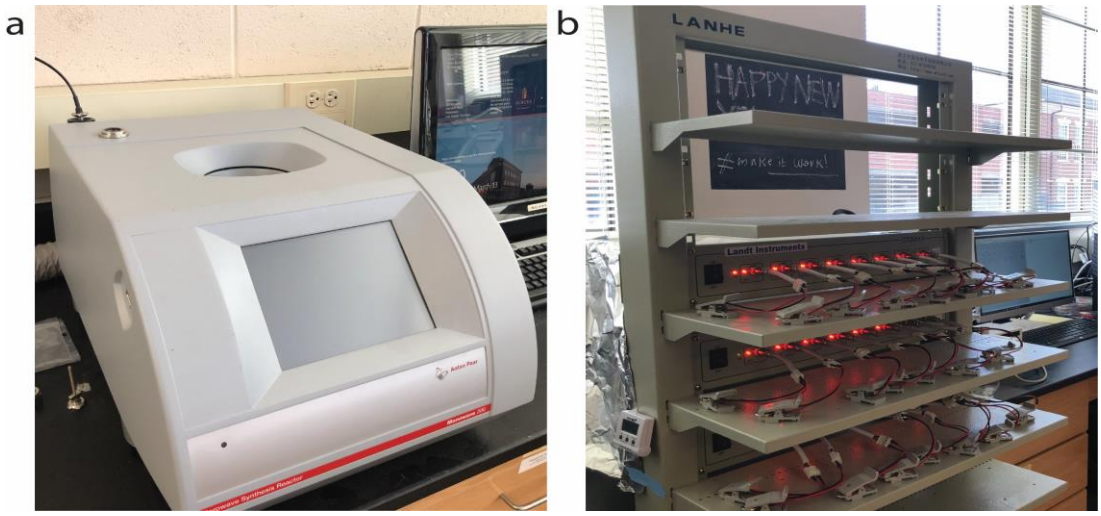

Fig.2.6 The equipment used for synthesis and characterization, (a) Mono-wave microwave reactor; (b) Landt battery cycling station.

Fig.2.7 The CR-2032 cell assembly components and casted anode material on the copper foil. Celgard separator, wave spring, coin cell cases and an assembled cell are also shown in the image.

Cyclic voltammetry (CV) tests were performed on a VMP3 Potentiostat at 0.2 mV $s^{-1,}$ and galvanostatic charge/discharge measurements at various current densities were performed on a multichannel battery cycling system (Landt, China, **Fig 2.1b**). The voltage window in all of the electrochemical measurements was set from 0.01 V to 3.5 V (vs. Li^+/Li). SnO_x/ $Ti_3C_2T_x$ samples' structure and morphology were characterized by using Bruker X-ray diffractometer (40 kV and 40 mA Cu-kα radiation), JEOL JSM-7000F scanning electron microscope (SEM) equipped with an energy dispersive spectrometer (EDS). The atomic force microscope (AFM) analysis was performed using Park Instruments NX10 AFM with a non-contact mode cantilever. Transmission Electron Microscopy (TEM) samples were prepared by drop casting diluted hybridized solutions on TEM grids.

2.4 Result and discussion

2.4.1 SnO_x/ $Ti_3C_2T_x$

Table 1 summarizes different reaction conditions that were used to synthesis $SnO_x/Ti_3C_2T_x$ samples:

Table 1: Sample synthesis condition (solution was 3:1 volume ratio EG/water).

Reaction Time $SnCl_2$:$Ti_3C_2T_x$ (wt%)	2 min	5 min	10 min	20 min
Pure $Ti_3C_2T_x$	○		○	
1:10			○	
1:1			○	
5:1		○	○	
10:1		○	○	○
20:1			○	

Although SnO_2 is a promising anode material, the disadvantage from its structure limits its application as stable and reliable electrode material in lithium-ion batteries.[43] So that the aim of this research is proved a stable carrier to SnO_2. The synthesised material is as presented in **Fig. 2.2a**, it is a black suspension, those fine particles can separate well from the reaction solution by centrifugal in few minutes. It is worth mentioning that there is some yellow-white powder also formed in the synthesis process as the reactant weight ratio of reactant $SnCl_2$: $Ti_3C_2T_x$ increased (**Fig. 2.2b**). Because of the deposited tin oxide, precise weight of each component cannot be

measured, so to best describe the samples we use the reaction weight ratio of $SnCl_2$: $Ti_3C_2T_x$. After synthesizing the hybrid materials, the suspension was transferred to the centrifugal tube to remove EG followed by washing the particles by DI water for several times before filtering.

Fig. 2.8 $SnO_x/Ti_3C_2T_x$ suspension (a) The 10- $SnO_x/Ti_3C_2T_x$ in microwave container; (b) sediment from 20- $SnO_x/Ti_3C_2T_x$ after centrifugal in 3500 rmp.

The final $SnO_x/Ti_3C_2T_x$ hybrid was dried in a vacuum oven.

Several characterization methods were used to study the structural details of the synthesized particles. Several characterization results are shown in **Fig.2.4**. With the XRD characterization given in **Fig.2.4a**, $Ti_3C_2T_x$ peaks at 2θ= 9.08°, 29.6°, and 33.9° confirms that hydrothermal method treated Ti_3C_2Tx still maintains its structure. For the SnO_2 deposited $Ti_3C_2T_x$ samples, as the $SnCl_2$: $Ti_3C_2T_x$ weight ratio increases from 1:10, 1:1, 10:1, the characteristic peaks of SnO_2 ((1 1 0) and (1 0 1) peaks) become stronger and more prominent, and on the contrary the characteristic (0 0 2) plane peak of $Ti_3C_2T_x$ becomes weaker. Also, samples with the weight ratio of 10:1 $SnCl_2$:$Ti_3C_2T_x$, have XRD profiles very close to SnO_2 XRD profile. This is thought to be the result of SnO_x formation in the $Ti_3C_2T_x$ mixture solution, confirming tin oxide formation within the MXene sheets. Besides, the XRD characterization result of samples with 5 min reaction time 10-SnO_x/ $Ti_3C_2T_x$ and 10 min reaction one is very similar; suggesting that the deposited SnO_x amount in those two samples are close.[44] Another item worth to mention with regard to the XRD

results is the extra peak in the tin oxide profile, which shows a different tin oxide structure formed in the process. Thus, hybrid material was named as $SnO_x/Ti_3C_2T_x$ as the tin oxide particles might have different compositions and structures.

AFM was used to image the MXene surface and the deposited particles after the hydrothermal reaction. In **Fig 2.4b**, the thickness of pure $Ti_3C_2T_x$ sheets before the reaction is shown to be about 2 nm and has a smooth surface which is similar to earlier reports.[20] However, the microwave reacted 1-10-SnO_x/ $Ti_3C_2T_x$ has a rough surface since the SnO_x is thought to be deposited on the surface. The variation of thickness on MXene sheets suggests that 1-10-SnO_x/ $Ti_3C_2T_x$ sample is formed with restacking of multiple 2D material layers and nanoparticles. The nanoparticles shown to be deposited on MXene surfaces are likely to be TMOs (TiO_2, SnO, and SnO_x) observed in XRD characterization. AFM study also suggests that the proposed TMO/MXene hybrid material is successfully synthesized. The shown structure and morphology represent nanosheets loaded nanoparticle, which originated from the in situ synthesis of tin oxide on $Ti_3C_2T_x$ surface.

More structural details of the synthesized SnO_x/ $Ti_3C_2T_x$ are given in the SEM images. From **Fig. 2.4d** to **Fig. 2.4i**, shown particles are treated at 180℃ in 850 W by microwave reactor. SEM image of Pure $Ti_3C_2T_x$ after microwave treatment for 2 min, is shown in **Fig. 2.4d**. The SEM images confirm that pure $Ti_3C_2T_x$ still has a layered structure. **Fig. 2.3e** also shows microwave treated $SnCl_2$ particles which are expected to be oxides. This further confirms that the reaction conditions are suitable both for synthesizing SnO_x and avoiding the MXene structure deterioration. In the **Fig.2.4f** to **Fig. 2.4h**, the weight ratio of $SnCl_2$: $Ti_3C_2T_x$ increases from 1:10, 1:1 to 10:1, with more loaded SnO_x particles, hybrid material roughness seems to be increasing. SnO_x/ $Ti_3C_2T_x$ samples synthesized in 10 minutes still maintain the layered structure. In **Fig. 2.3i**, 5 min 10-SnO_x/ $Ti_3C_2T_x$ has a similarly high amount SnO_x formation on the edges of MXene particles, and there is not a significant visual difference in 10-SnO_x/ $Ti_3C_2T_x$ and 5-SnO_x/ $Ti_3C_2T_x$, which needs further characterization.

TEM images of the 5 min 10-SnO_x/Ti_3CT_x sample are given in **Fig .2.5(a-d)**. TEM analysis further confirms that the structure of hybrid material is composed of metal oxide nanoparticles deposited on MXene sheets. In the **Fig.2.5d**, the average lattice distance of surface deposited transition metal oxide is about 0.34 nm. The SnO_2 lattice space is reported to be about 0.333 nm.[45] The XRD spectra are shown in **Fig. 2.6.a**, a clear peak of SnO2 (110) plane can be observed.

Corresponding lattice parameter is calculated from Bragg's equation, which is about 0.3459 nm. Due to the aforementioned observations and analysis, it can be concluded that the material synthesized within $Ti_3C_2T_x$ sheets is mainly SnO_2. EDS analysis results are shown in **Table.2**, also indicates the hybrid material includes the tin oxide.[46]

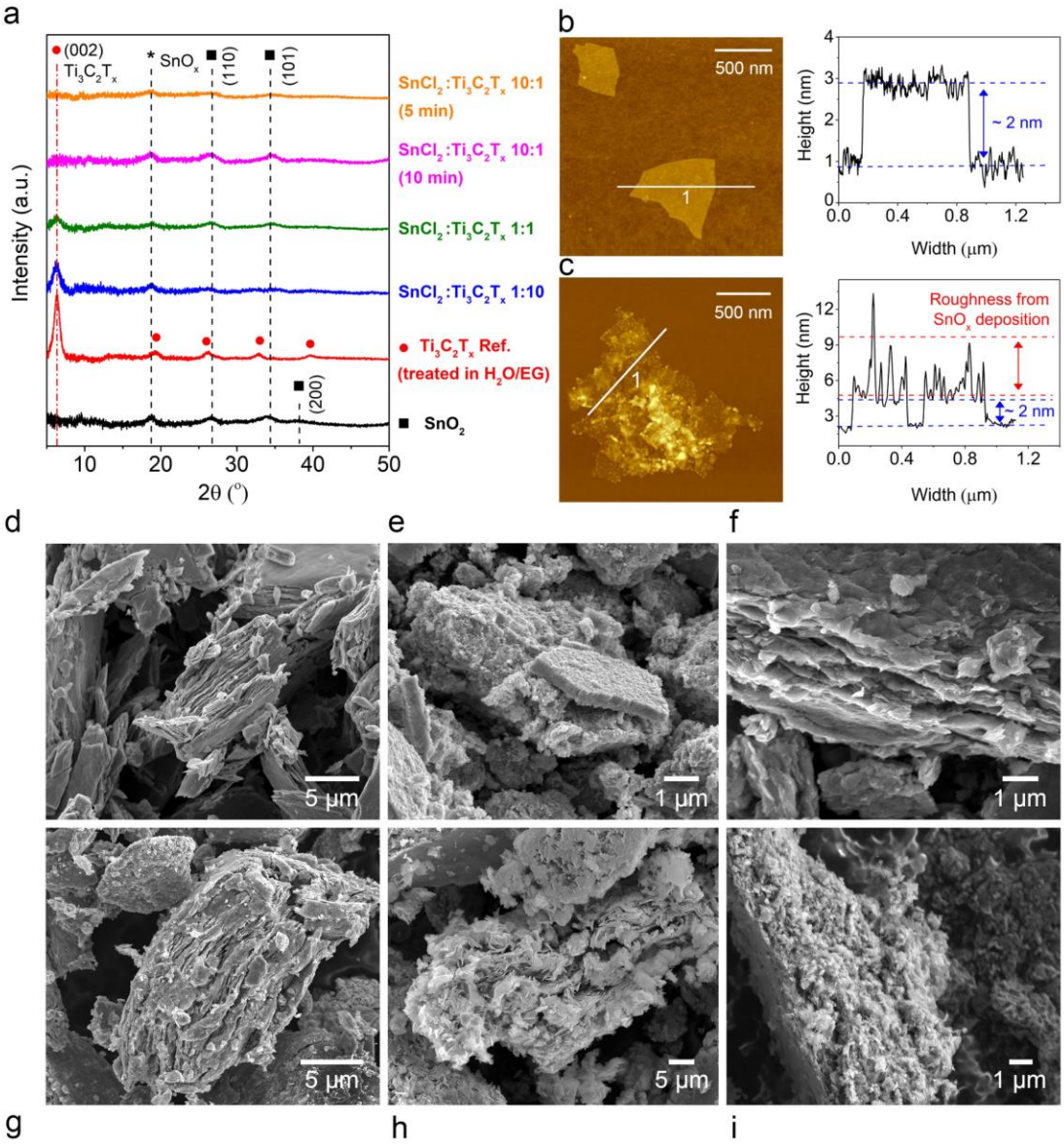

Fig.2.9 Characterization images of (a) X-ray diffraction (XRD) patterns of different $SnCl_2$ to $Ti_3C_2T_x$ ratios. (b) Atomic force microscopy (AFM) image and the corresponding height profile of $Ti_3C_2T_x$ flakes and (c) $SnCl_2$ to $Ti_3C_2T_x$ ratio of 1:10 with 10 minutes reaction time. The low loading of tin precursor was used to elaborate on AFM sample preparation and imaging. These images clearly show the deposition of nanostructured SnO_x on the surface of $Ti_3C_2T_x$ nanosheets. SnO_x SEM images of (d) $Ti_3C_2T_x$ treated in H_2O/EG, (e) pure SnO_x, and (f-i) 1:1 (10 min), 5:1 (10 min), 10:1 (10 min), and 10:1 (5 min) $SnCl_2$ to $Ti_3C_2T_x$, respectively.

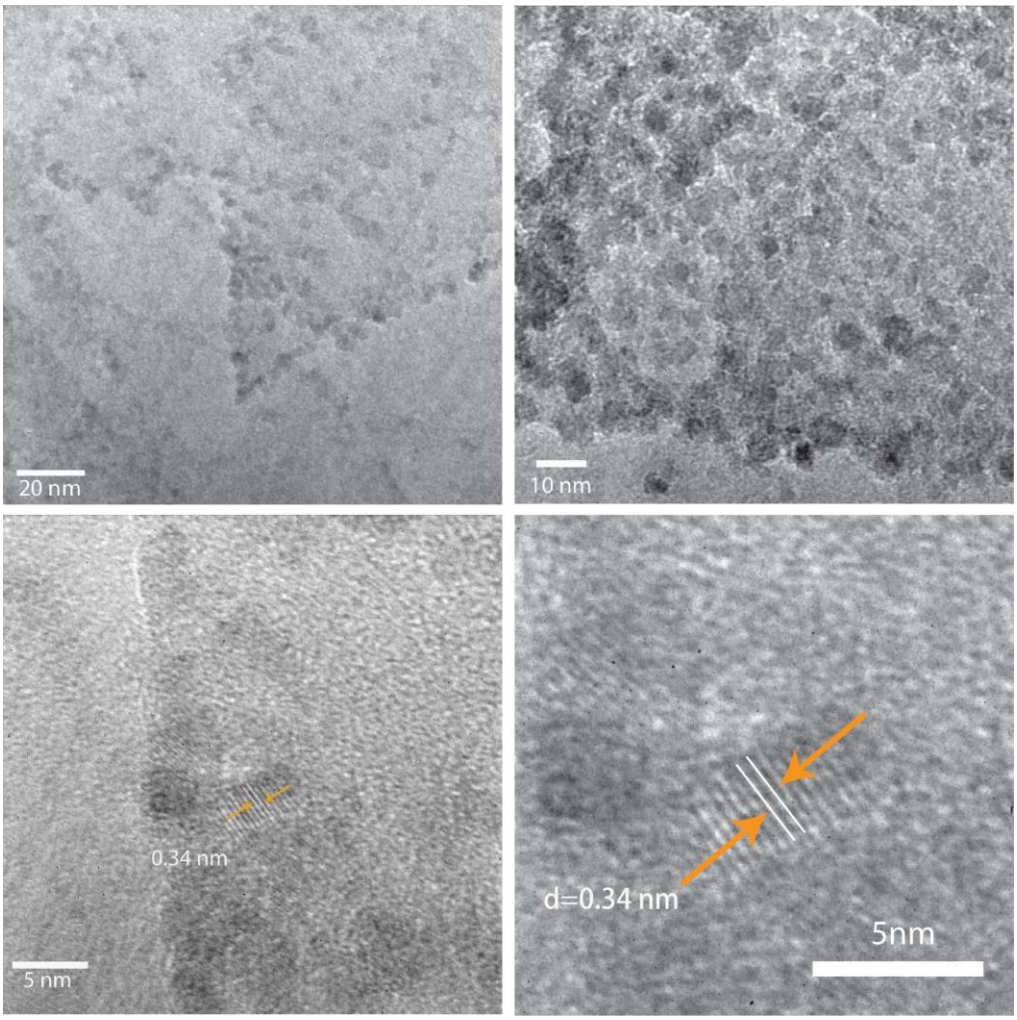

Fig.2.10 TEM image in 5 min 10-$SnO_x/Ti_3C_2T_x$ sample at different magnifications (a-d).

Table 2. Elemental distribution of 5 min 10- $SnO_x/Ti_3C_2T_x$ sample.

Element	Weight %	Atomic %
C K	24.11	62.85
O k	2.84	5.57
Sn L	27.15	7.16
Ti k	11.21	7.33

In the reaction process, the EG is used as a stabilizing agent in solution to protect $Ti_3C_2T_x$ from oxidizing and thus, improving the electrochemical performance. To confirm this idea, MXene solution with EG and without EG is prepared (3:1 EG: Water) and treated in a microwave reactor under the same conditions. The XRD spectra are shown in **Fig. 2.6b** highlights the change in the peak intensity corresponding to (002) plane of MXene structure. MXenes treated in pure water showed a weaker (002) plane peak compared to the MXene treated in EG/water mixture solution sample, showing that EG works as a stabilizer in the reaction process.

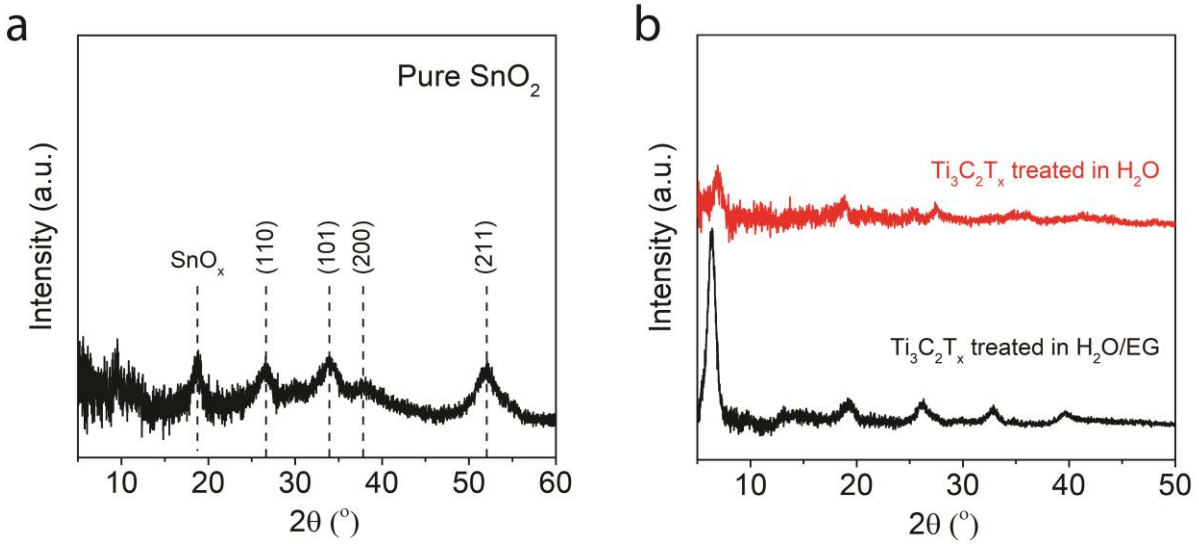

Fig.2.11 XRD image of (a) synthesized particle with $SnCl_2$ solution in microwave reactor;(b) $Ti_3C_2T_x$ in two types of reaction solution.

To find out the effect of above mentioned two different reaction environments, pure water and 3:1 EG/water, on the electrochemical performance of synthesized $SnO_x/Ti_3C_2T_x$, a cycle performance test was performed (**Fig.2.7)**. At 50 mA g^{-1} current density, cycling performance of two 10 min 10-$SnO_x/Ti_3C_2T_x$ samples is shown. The sample synthesized in EG/water environment has a mass loading of ~0.99 mg cm^{-2}, while the sample synthesized in pure water environment has a mass loading of ~1.17 mg cm^{-2}. Their specific capacities are 543.7mAh g^{-1} and 479.7 mAh g^{-1}, respectively. As the specific capacity of the latter electrode showed an unstable/decreasing trend, fabrication of electrodes are limited to solutions treated with EG and water mixture.

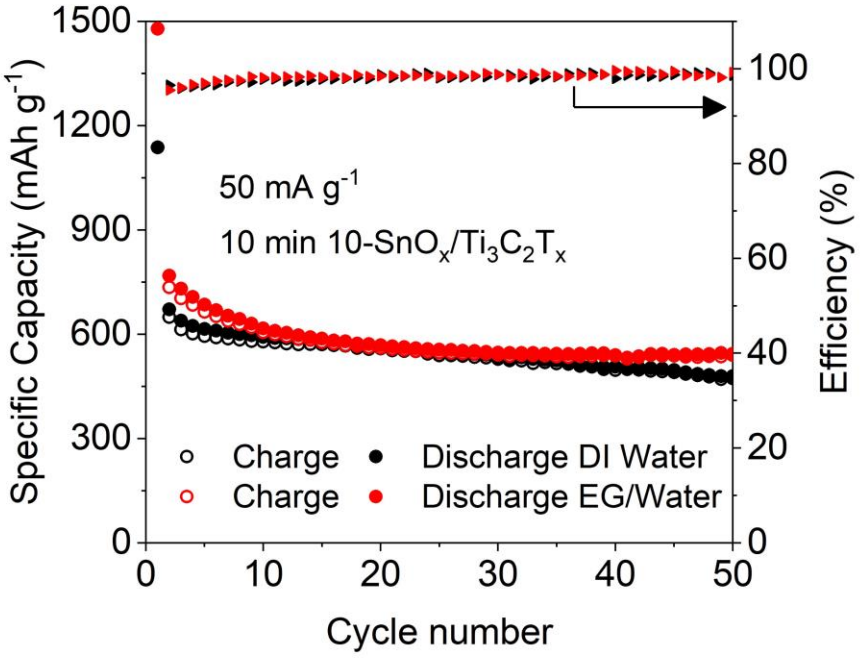

Fig. 2.12. 50 cycles of 10 min 10- $SnO_x/Ti_3C_2T_x$ synthesis in water and EG/water environment.

The CV curves in **Fig 2.8a** includes profiles of 10-$SnO_x/Ti_3C_2T_x$, 5-$SnO_x/Ti_3C_2T_x$, and $Ti_3C_2T_x$ film. The working voltage window is set to be between 0.01 and 3.00 V (vs. Li/Li^+), and it can be seen that energy storage capability of $SnO_x/Ti_3C_2T_x$ has significantly improved compared to the $Ti_3C_2T_x$ film. The CV profiles showed that increasing the amount of deposited SnO_x, improves electrochemical performance since the area under the curve of 10-$SnO_x/Ti_3C_2T_x$ is larger than 5-$SnO_x/Ti_3C_2T_x$. Combining with material characterization results, the difference between the CV profiles of pure $Ti_3C_2T_x$ and hybrid material arises from the deposited tin oxide particles. In **Fig 2.8b**, CV curves of 10 min 10-$SnO_x/Ti_3C_2T_x$ are presented. Firstly, it is hypothesized that cathodic peaks at 0.65 and 1.2 V, are as the result of SEI layer formation and lithium salt-based electrolyte ($LiPF_6$/EC-DEC) reducing tin oxide into metal Sn; these reactions are shown with the equations (I) and (II). The significant reduction peaks around 0.38 to 0.87 V represent the formation of Li_xSn ($0 \leqslant x \leqslant 4.4$) which is shown with equation (2), and its reversible equation is given as equation (3). This is thought to be the lithium storage mechanism

of this composite anode.[44,47,48] Except the intercalation with tin oxide; the Li^+ can also intercalate into $Ti_3C_2T_x$ to form $L_xTi_3C_2$ as equation (1) and (4) shows. This result reflects the mechanism of SnO_x lithium-ion storage in the LIBs, and since its majority of lithium-ion stored in this hybrid material is SnO_x, higher SnO_x loading is expected to deliver higher specific capacity. Consistent CV profiles of 10-$SnO_x/Ti_3C_2T_x$ over cycling shown in **Fig.2.8b** indicates the good reversibility of this hybrid anode material.

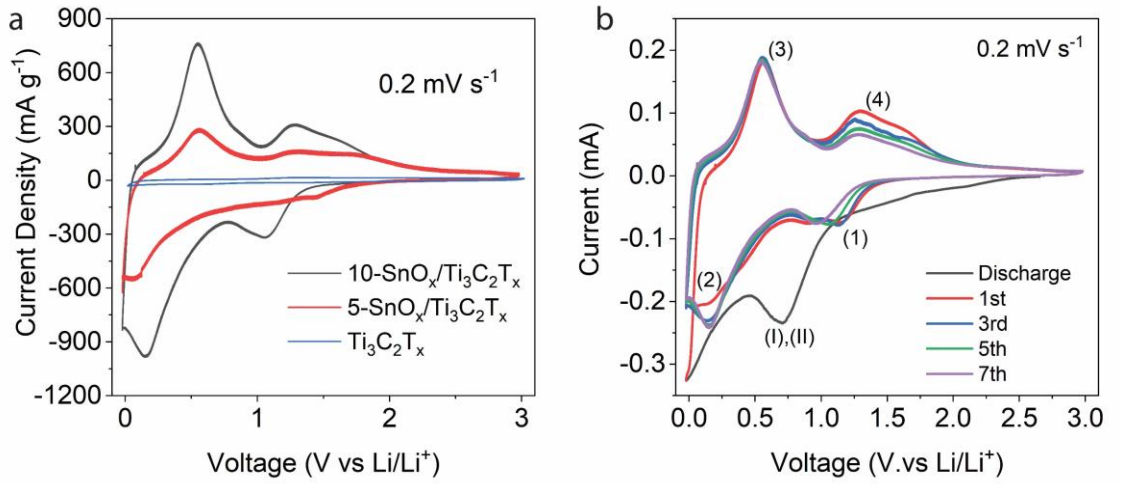

Fig. 2.13 CV curve at 0.2 mV s^{-1} scan rate of (a) 5-SnO_x/ $Ti_3C_2T_x$,10- SnO_x/ $Ti_3C_2T_x$ and pure $Ti_3C_2T_x$ at same cycle number; (b) 10- $SnO_x/Ti_3C_2T_x$ cycling performance.

$$SnO + 2Li^+ + 2e^- \rightarrow Sn + Li_2O \quad \text{(I)}$$

$$SnO_2 + 4Li + 4e^- \rightarrow Sn + 2Li_2O \quad \text{(II)}$$

$$Sn + xLi^+ + xe \leftrightarrows Li_xSn\ (x \leq 4.4) \quad (2)(3)$$

$$Ti_3C_2T_x + xLi^+ + x4e^- \leftrightarrows Li_xTi_3C_2 \quad (1)(4)$$

To find the optimum reaction conditions and the weight ratio of $SnO_x/Ti_3C_2T_x$, two possible verified factors that may affect the electrochemical performance were tested. First, the ratio between $SnCl_2$ and $Ti_3C_2T_x$ was changed to make 1-10-$SnO_x/Ti_3C_2T_x$, 5-$SnO_x/Ti_3C_2T_x$, 10-$SnO_x/Ti_3C_2T_x$ and 20-$SnO_x/Ti_3C_2T_x$. Their specific capacities in 50 mA g^{-1} current density were 192.6, 390.5, 721.9 and 731.2mAh g^{-1} at their 100^{th} cycles, respectively. The increase in the

values of specific capacities clearly indicates that adding more $SnCl_2$ reactant would increase the specific capacity of the synthesized material. However, the electrode electrochemical performance at the weight ratio of 10:1 $SnCl_2$: $Ti_3C_2T_x$ did not show a significant improvement. Possible reasons might include, higher amounts of impurity with higher amounts of $SnCl_2$ addition, (**Fig. 2.3b**) or a limitation on the SnO_x deposition on MXene flakes. For further studies 10:1 $SnCl_2$: $Ti_3C_2T_x$ weight ratio was kept as the optimum value in the synthesis procedure.

With the weight ratio kept constant, the effect of reaction time was also investigated by changing the reaction time from 5 minutes, to 10, 15, and 20 minutes. After 150 cycles in 50 mA g^{-1}, the specific capacity of 5 min, 10 min, 15 min, and 20 min 10-$SnO_x/Ti_3C_2T_x$ samples were 852.2, 721.9, 585.4 and 567.3 mAh g^{-1}, respectively. The specific capacity differences between various electrode materials are presented in **Fig.2.9b**. The decrease in specific capacity as the reaction time increases reflects the negative impact of longer reaction time on the MXene flakes. Results indicated that increasing the reaction time might cause $Ti_3C_2T_x$ to oxidize more, resulting in reducing the active surface area for deposition reaction, which in turn results in a lower amount of deposited SnO_x nanoparticles. It can be concluded that reducing microwave reaction time leads to a more stable anode material and increasing $SnCl_2$: $Ti_3C_2T_x$ ratio can increase the SnO_x deposition which increases the electrochemical performance of the electrodes. Our results show that the best electrochemical performance was obtained with 5 min reaction time for 10:1 ratio $SnO_x/Ti_3C_2T_x$.

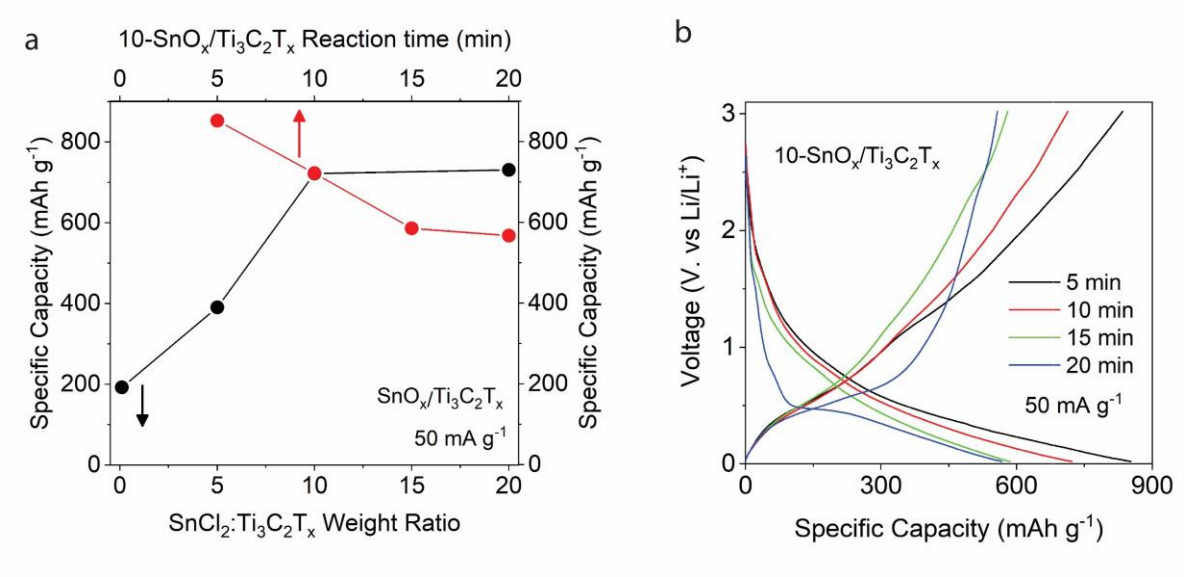

Fig. 2.15 Dependence of the electrochemical performance on various factors. (a) Weight ratio and specific capacity of SnO_x/ $Ti_3C_2T_x$ in 50 mA g^{-1} current density ;(b) The effect of reaction time on the charge/discharge profile of 10-SnO_2/ $Ti_3C_2T_x$ samples.

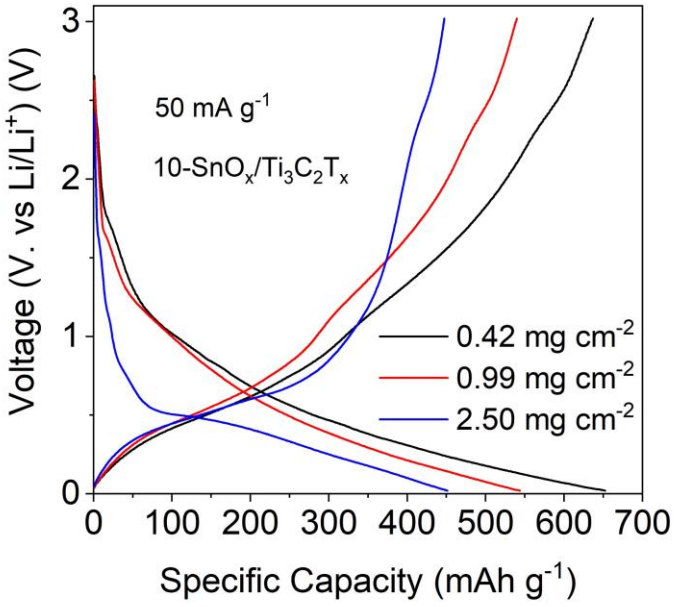

Fig.2.14 Specific capacity of electrode with different mass loadings (a) 0.42; (b)0.99 and (c) 2.50 mg cm^{-2}.

As can be seen in **Fig. 2.10**, the mass loading of the electrodes is another factor affecting the anode material electrochemical performance. 10-$SnO_x/Ti_3C_2T_x$ sample with a 10-minute reaction duration is coated on copper with different thicknesses, meaning different mass loadings which are 0.42, 0.99 and 2.50 mg cm^{-2} for 7 mm diameter foil. The specific capacities of each sample are about 652.5, 543.7 and 451.2 mAh g^{-1} in the 50^{th} cycle, respectively. The sample with the highest mass loading has the lowest specific capacity since the thickness of the hybrid material may block the diffusion of ions and cause a decrease in the electrical conductivity for the sample.

To compare the electrochemical performances of pure $Ti_3C_2T_x$ film and 5 min, 10-$SnO_x/Ti_3C_2T_x$ samples, both samples are tested under the same conditions (at a scan rate of 50 mA g^{-1}). As shown in **Fig. 2.11**, the pure $Ti_3C_2T_x$ anode, compared to the 5 min $SnO_x/Ti_3C_2T_x$ (mass loading about 0.45 mg cm^{-2}) gives much lower specific capacity at a scan rate of 50 mA g^{-1}. After running 500 cycles, the MXene film has a specific capacity in 98.1 mA g^{-1}, but the specific capacity of 5 min 10-$SnO_x/Ti_3C_2T_x$ rises to 1274.0 mAh g^{-1}, which shows the effect of deposited SnO_x nanoparticles and indicates that this modification is helpful to improve specific capacity. The $SnO_x/Ti_3C_2T_x$ anode also gives an interesting result since the composite material has a similar specific capacity rising phenomenon like MXene material shows. Firstly, this indicates that the flexibility and electrochemical properties of two-dimensional MXenes are maintained after the microwave treatment. Also, the reason causing this phenomenon may be the intercalated ions increasing the layer lattice distance.[19] Since the used material in this study is delaminated $Ti_3C_2T_x$, and they are aggregated during the hybrid material synthesis process, the overall specific area of the final product may be decreased since nanosheets overlap. However, during charging and discharging, nanosheets get separated again, leading to better electrochemical performance since the number of lithium interaction sites are increasing. To prove this assumption, further characterization of hybrid material is needed.

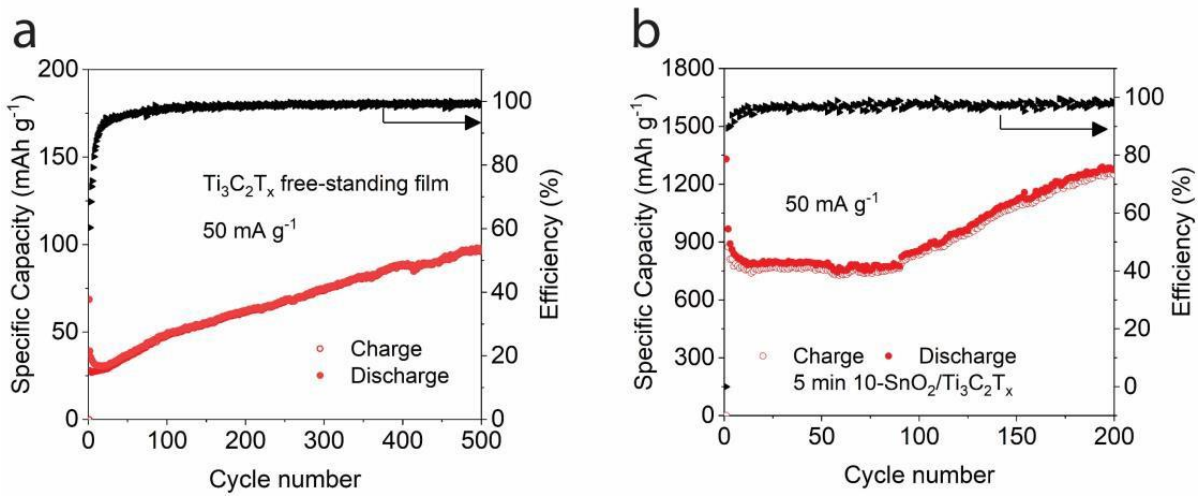

Fig.2.16. Electrochemical performances of different electrode materials at a scan rate of 50 mA g^{-1}. (a) Free-standing $Ti_3C_2T_x$ film; (b) 5 min SnO_x/ $Ti_3C_2T_x$.

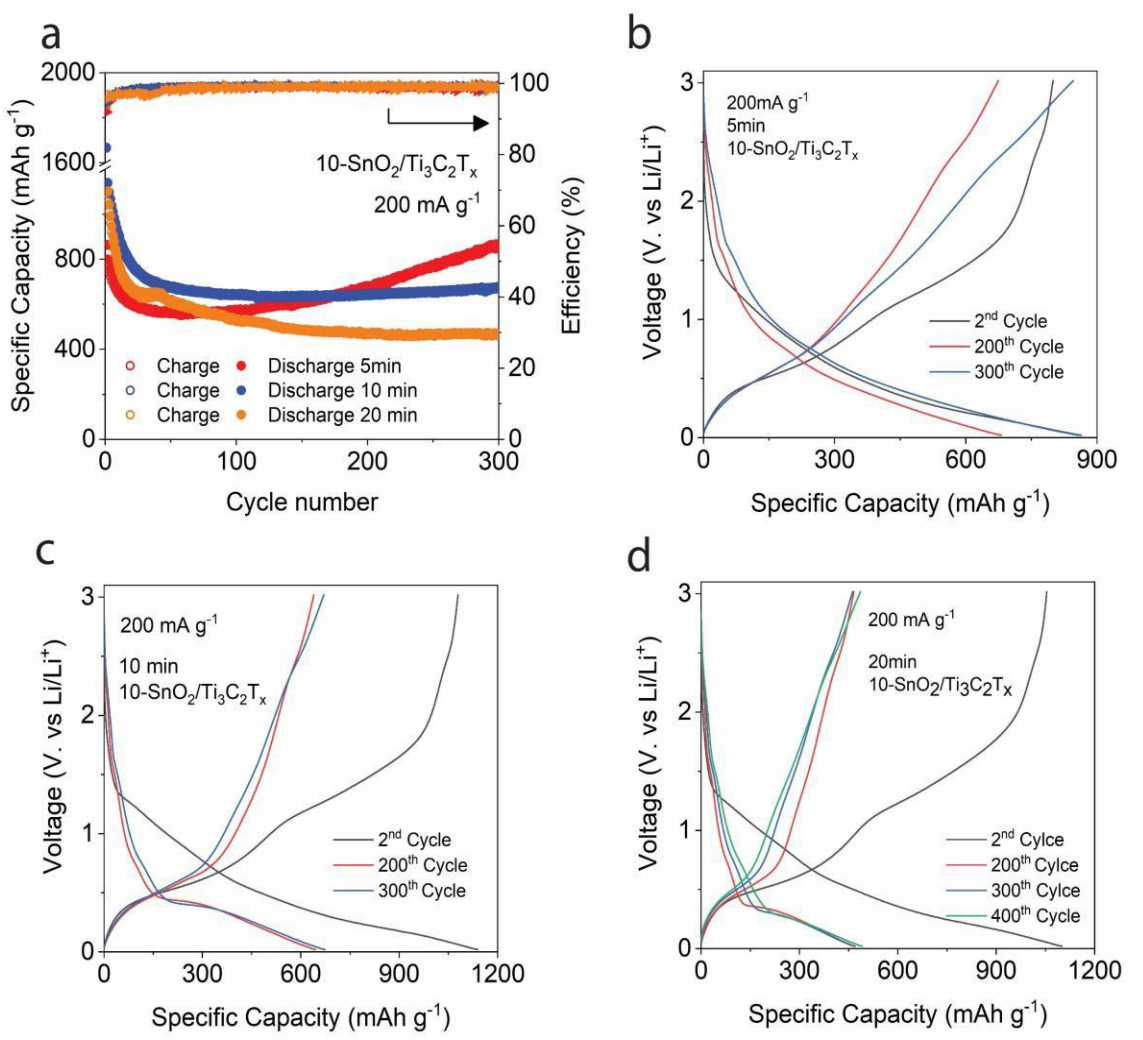

Fig.2.17 Effects of the reaction time to electrochemical performance. (a) Capacity retention of 10-SnO_x/ $Ti_3C_2T_x$ samples with 5 min, 10 min and 20 min reaction time, at 200 mA g^{-1}; (b-d) Galvanostatic charge-discharge curves of 10-SnO_x/ $Ti_3C_2T_x$ of 5 min, 10 min, 20 min reaction time, respectively.

To understand the impact of higher current density in 10-SnO_x/$Ti_3C_2T_x$, three samples with different reaction durations were tested at 200 mA g^{-1} scan rate. The long-term cycle performance of 5 min, 10 min and 20 min 10-SnO_x/$Ti_3C_2T_x$ under 200 mA g^{-1} current density is shown in **Fig.2.12a**. The samples in **Fig.2.12a** have good capacity retention and capacity recovery over time. The 5 min SnO_x/$Ti_3C_2T_x$ has a much better performance than the other two

samples as the number of cycles increases. After the 300th cycle, the specific capacity of 5 min, 10 min, and 20 min 10-$SnO_x/Ti_3C_2T_x$ samples become, 858.8 mAh g^{-1}, 673.4 mAh g^{-1}, and 467.6 mAh g^{-1}, respectively. Unlike the pure SnO_x anode, the hybrid material has good stability and capacity retention. It has a high coulombic efficiency, which is close to 100%. **Fig. 2.12b** through **Fig.2.12d** show a more detailed comparison of the sample's performance at different cycle numbers. The specific capacity of 5 min 10-$SnO_x/Ti_3C_2T_x$ almost recovered to the 2nd cycle's capacity after the 300th cycle, but the long-time reaction samples' capacity recovery, especially the 20 min reacted 10-$SnO_x/Ti_3C_2T_x$, is not as obvious as the shorter time reaction samples. The long-reaction time sample only shows a slight specific capacity recovery after 400 cycles (**Fig.2.12c** and **Fig.2.12d**), and it has a specific capacity of 467.6 mAh g^{-1} at 300th cycle and 492.0 mAh g^{-1} at 400th cycle. This result shows the impact of increasing the reaction time; the open structure of MXene becomes inhibited after some time, and the interlayer space becomes harder to enlarge, which decreases the specific capacity.

The rate capability test results show that 10-$SnO_x/Ti_3C_2T_x$ has good performance under a range of current densities. In Fig. **2.13a**, the 10 min, 10-$SnO_x/Ti_3C_2T_x$ has a stable cycling performance with high coulombic efficiency and high specific capacity under 50 mA g^{-1} for 200 cycles. The specific capacity is 999.4 mAh $g^{-1,}$ and after finishing the cycling test, the same cell was tested under different current densities of 100, 200, 500, 1000 and 50 mA g^{-1} (shown in **Fig. 2.13b**) and the valued of specific capacities are 971.3, 751.9, 432.5, 281.3, and 1025.0 mAh g^{-1} after the current density reduces to 50 mA g^{-1}. The increasing trend of specific capacity after the current density is reduced to 50 mA g^{-1} suggests that the capacity of hybrid material continues to increase even after the current density change. Comparing the specific capacities at 200 mA g^{-1} and 500 mA g^{-1}, the capacity decrease is about 42.48%, which means the long

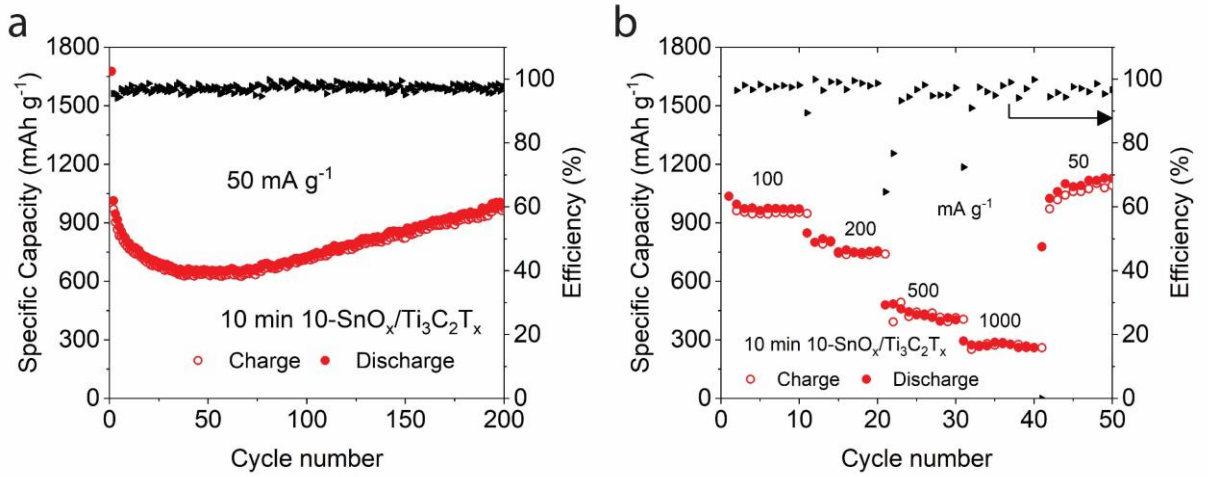

Fig.2.18 10 min 10- SnO_x/ $Ti_3C_2T_x$ performance of (a) Long-term electrochemical performance of 10 min 10- SnO_x/ $Ti_3C_2T_x$ at 50 m g^{-1}. (b) The step ability test of 10 min 10- SnO_x/ $Ti_3C_2T_x$ under 50, 100, 200, 500, 1000 and 50 mA g^{-1}.

reaction time sample is not good to work under high current density conditions.

The rate capability test results for 5 min 10-SnO_x/$Ti_3C_2T_x$ sample is shown in **Fig. 2.14a.** The current density steps through 50, 100, 200, 500, 1000 and returns to 50 mA g^{-1} with specific capacity 748.4, 677.2, 600.7, 520.6, 455.2, 671.9 mAh g^{-1}, respectively. After reducing the current density, the specific capacity recovers to 89.78% initial value. After finishing the test, in **Fig.2.14b**, the sample tested again at 2A g^{-1} current density to measure the performance of SnO_x/$Ti_3C_2T_x$ at a very high current density, and its specific capacity calculated to be 430.4 mA h g^{-1}. The results show that electrode structures interlayer distance may be increasing with the intercalation and deintercalation of ions. In another high current density test, another 5 min 10-SnO_x/$Ti_3C_2T_x$ sample also had a specific capacity rising as presented in **Fig. 2.15**, and its capacity recovers to 583.7 mAh g^{-1} after 500 cycles at 500 mA g^{-1} with mass loading about 0.76 mg cm^{-2}.

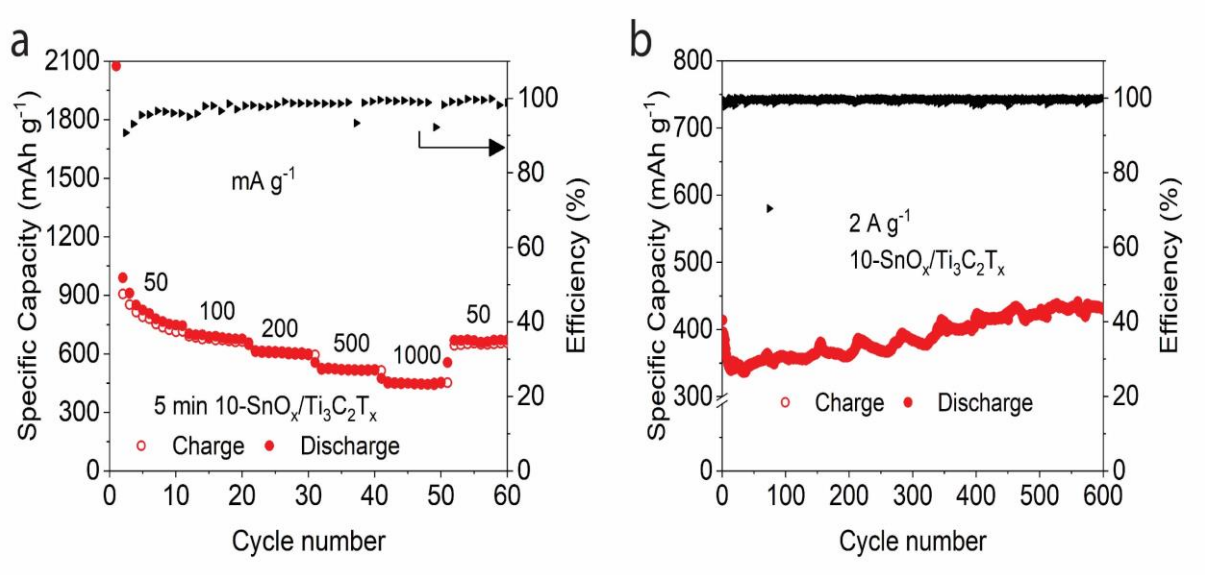

Fig. 2.19 5min 10- SnO_x/ $Ti_3C_2T_x$ electrochemical performance under 500 mA g^{-1} of (c) 10 min; (d) long time cycle performance in 2A g^{-1}.

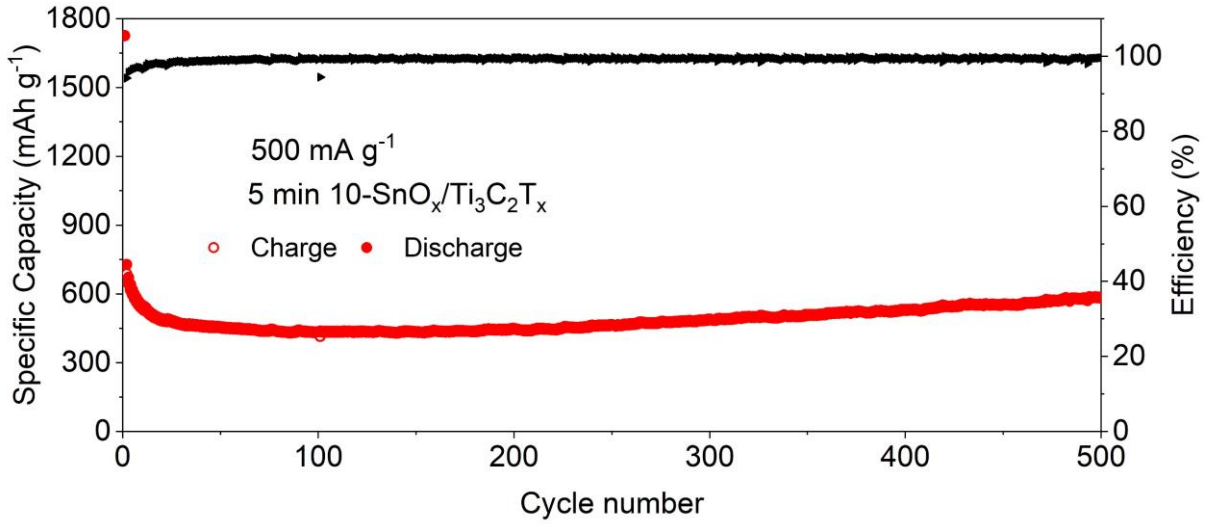

Fig. 2.20 Long cycle performance of 5 min 10-SnO_x/ $Ti_3C_2T_x$ under 500 mA g^{-1}.

To test whether this capacity recovery phenomenon is exhibited by samples with other reaction times, 10 min 10-SnO_x/$Ti_3C_2T_x$ in a similar mass loading is used to making a long cycle

performance test, and the result is shown in **Fig. 2.16a**. After the 600th cycle, its specific capacity is 505.8 mAh g^{-1} while the 200th cycle's specific capacity is 366.1 mAh g^{-1}, which means the specific capacity rising for 10 min $SnO_x/Ti_3C_2T_x$ sample doesn't happen even as the cycle number keeps increasing. The shape of the long-term cycle performance profile shows the specific capacity drops with an increased number of cycles. This result may be caused by crystal instability or even deterioration in the electrode's working process. The other 10 min 10-$SnO_x/Ti_3C_2T_x$ sample was tested in 500 mA g^{-1} with higher mass loading and exhibited a similar result. The specific capacity in the 200th cycle is 461.1 mAh $^{-1,}$ and it becomes 433.8 mAh g^{-1} after the 600th cycle (shown in **Fig. 2.16b**). This can be evidence that the longer reaction time has some impact on the 10-$SnO_x/Ti_3C_2T_x$ crystal structure that reduces its storage ability.

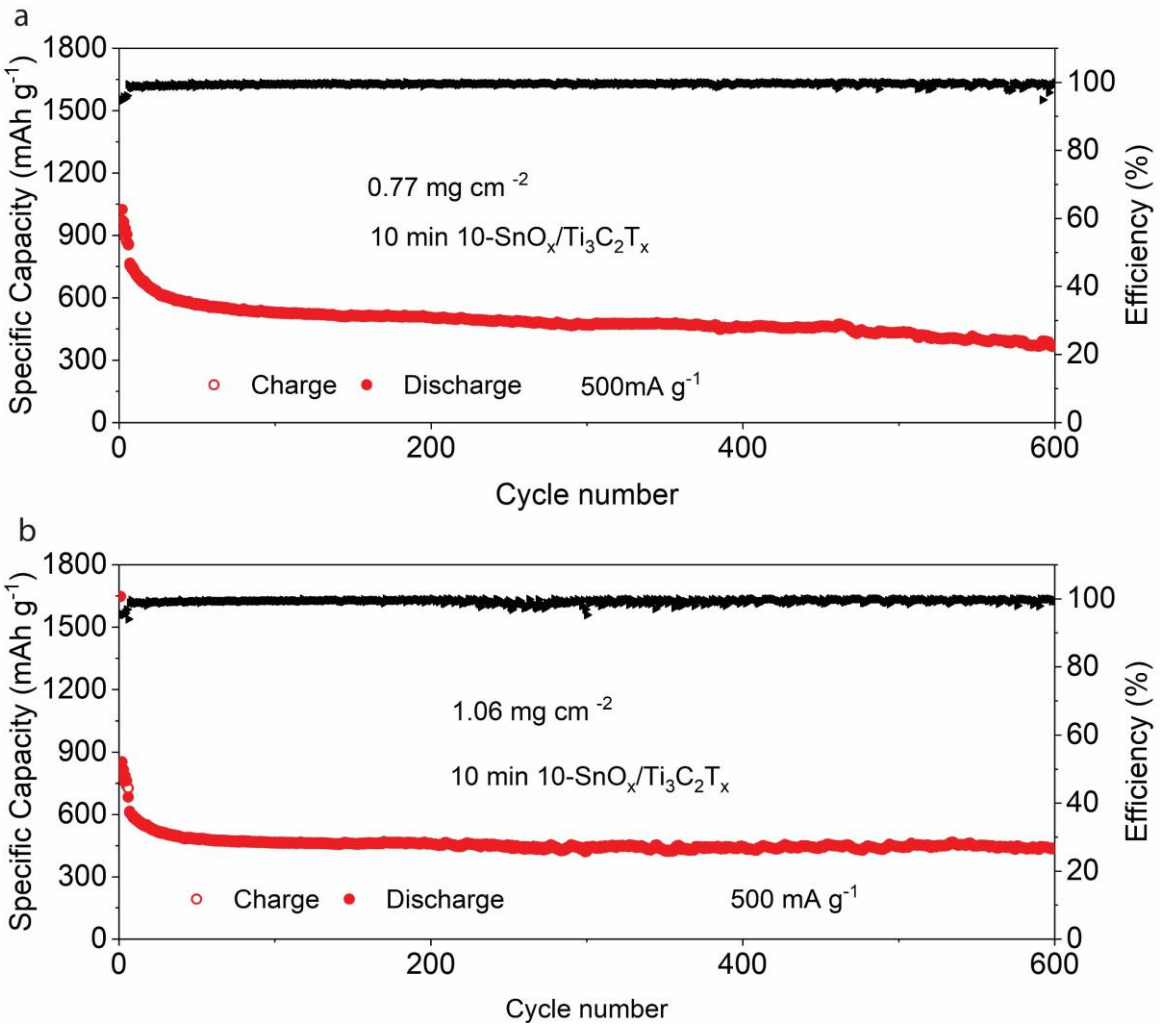

Fig. 2.21 Long cycle performance of 10 min 10-$SnO_x/Ti_3C_2T_x$ under 500 mA g^{-1} in mass loading (a)0.77 mg cm^{-2} and (b) 1.06 mg cm^{-2}.

The Comparison of 10-$SnO_x/Ti_3C_2T_x$ made in this research with some earlier Sn-C materials specific capacity is given in **Table 3**. Under various current densities, 10-$SnO_x/Ti_3C_2T_x$ has better performance, and it proves the advantage of the microwave assisted electrode synthesis method, which can be used to create a high specific capacity electrode material in a short time that maintains its intercalated structure.

Table 3 Electrochemical performance of different SnO_2-C or MXene anode material for LIBs

Name of material	Method	Synthesis condition	Current density mA g^{-1}	Specific capacity mAh g^{-1}	2D material treadment	Ref.
SnO_2/Ti_3C_2	ALD	150℃ Precursors (Sn^{4+} and O_3) alternative	500	258	Exfoliated Ti_3C_2 (LiF+HCL bath sonci)	47
SnO_2/Ti_3C_2	Tradition Hydrothermal	120℃ 50:9 wt% $SnCl_4.H_2O$: $Ti_3C_2T_x$,10 h	500	500	Delaminated Ti_3C_2 (LiF+HCL bath sonci)	44
SnO_2/Ti_3C_2	Tradition Hydrothermal	120℃ 50:9 wt% $SnCl_4.H_2O$: $Ti_3C_2T_x$,10 h	200	697	Delaminated Ti_3C_2 (LiF+HCL bath sonci)	44
SnO_x/Ti_3C_2	Tradition Hydrothermal	180℃ 1:1 wt% $SnCl_2.H_2O$: $Ti_3C_2T_x$, 6 h	500	430	Delaminated Ti_3C_2 (HF)	48
SnO_x/Ti_3C_2	Tradition Hydrothermal	180℃ 1:1 wt% $SnCl_2.H_2O$: $Ti_3C_2T_x$,6 h	200	450	Delaminated Ti_3C_2 (HF)	48
SnO_2/graphene /C	Hydrothermal and furnace heat	160℃ for 10 h for GO/$SnCl_2$/glucose 500 ℃ for 4 h heat	200	757	ultrasonica-tion exfoliated RGO	49
3DMCl	Microwave irradiate	20 s microwave irradiate fezzed dry Ti_3C_2/PVA in acetone ferrocene solution	500	161		50
$SnO_x/Ti_3C_2T_x$	Microwave Assistance	180℃ 10:1 wt% $SnCl_2.H_2O$: $Ti_3C_2T_x$ 5 min	500	437	Delaminated Ti_3C_2 (LiF+HCL Tip sonci)	This work
$SnO_x/Ti_3C_2T_x$	Microwave Assistance	180℃ 10:1 wt% $SnCl_2.H_2O$: $Ti_3C_2T_x$ 5 min	200	834	Delaminated Ti_3C_2 (LiF+HCL Tip sonci)	This work

2.4.2 Other TMO/$Ti_3C_2T_x$ performance

In the experiment, we also synthesized 10-MnO_2/$Ti_3C_2T_x$ and 1-MoO_3/$Ti_3C_2T_x$ as LIB anode materials through the same method and the same reaction conditions, and they have achieved good electrochemical performance. TMO/MXene material is tested under 50 mA g^{-1} and the synthesis time is two steps of 5 minutes (10 minutes total). In **Fig. 2.17**, the SEM image of 10-MnO_2/$Ti_3C_2T_x$, the layered structure of MnO_2 deposited $Ti_3C_2T_x$ particles. It can be seen that the MnO_2 like SnO_x, accumulated on the MXene edges and gives a relatively smooth surface. Since the applied microwave condition is exactly same to synthesized SnO_x/$Ti_3C_2T_x$, it means the microwave assisted hydrothermal method synthesis condition also fits other type TMO deposited hybrid materials, and it is not affected by applying transition metal salt reactant.

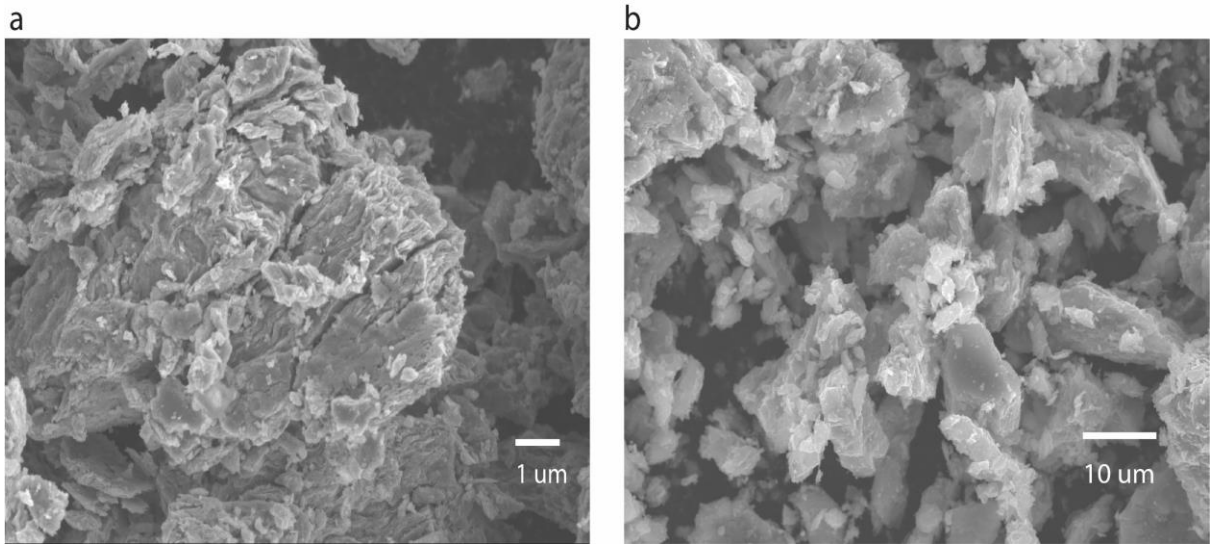

Fig.2.22 SEM image of 10-MnO_2/ $Ti_3C_2T_x$ in (a) 5000 amplification; (b) 1500 amplification.

In **Fig.2.18a** and **Fig.2.18b**, at 50 mA g^{-1} the long-term performance curve of 10-MnO_2/$Ti_3C_2T_x$ and 1-MoO_3/$Ti_3C_2T_x$ as LIBs anode gives specific capacity about 611.6 mAh g^{-1} and 362.0 mAh g^{-1}, respectively. This result shows this method has a high potential to achieve different types of TMO/$Ti_3C_2T_x$ since all those three types of material has a better performance

than the original pure MXene anode. The test result of $MnO_2/Ti_3C_2T_x$ and $MoO_3/Ti_3C_2T_x$ has a similarly stable cycle performance as a LIB's anode after 150 cycles and even shows capacity rising in $MnO_2/Ti_3C_2T_x$.

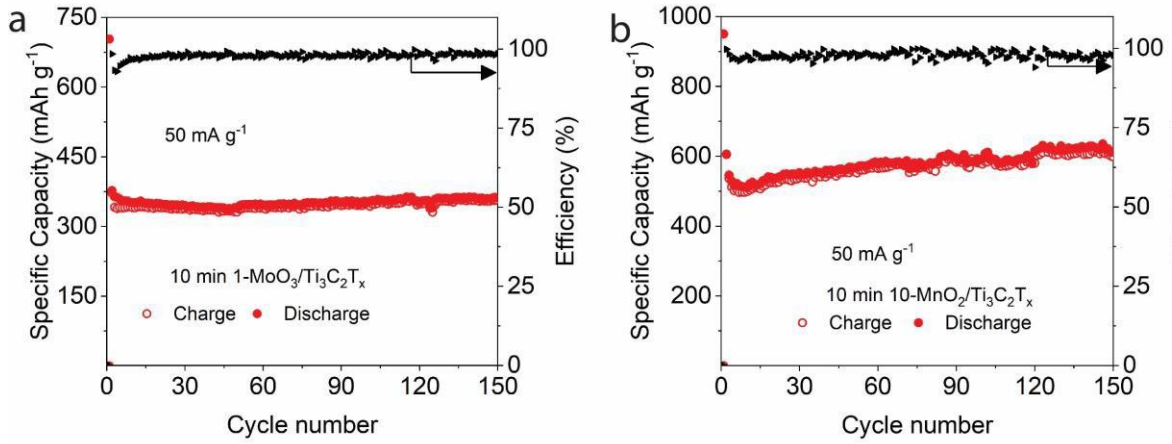

Fig. 2.23 Other types of TMO/ $Ti_3C_2T_x$ at 50 mA g^{-1} galvanostatic charge-discharge curves of (a) 10 min 1- MoO_3/ $Ti_3C_2T_x$ and (b) 10 min 10-$MnO_2/Ti_3C_2T_x$.

In **Fig. 2.19**, 10 min 10-$MnO_2/Ti_3C_2T_x$ can also be applied into the sodium-ion battery (SIB) andit gives a specific capacity about 260.5 mAh g^{-1} at the 1st cycle, and it has 121.2 mAh g^{-1} at the 65th cycle. The cell type is CR-2016, and the electrolyte is $NaClO_4$ in EC (ethylene carbonate)/PC (propylene carbonate) solution, and the assembly process is similarly as the CR-2032 cell. However, the unstable capacity rising between the 15th to 21st cycles could be a problem of side reactions happening during battery operation, which means there are some flaws of 10-$MnO_2/Ti_3C_2T_x$ as SIB's anode since its crystal structure maybe deforming during the test and causing battery damage. Understanding this instability still requires more sample synthesis and characterization work.

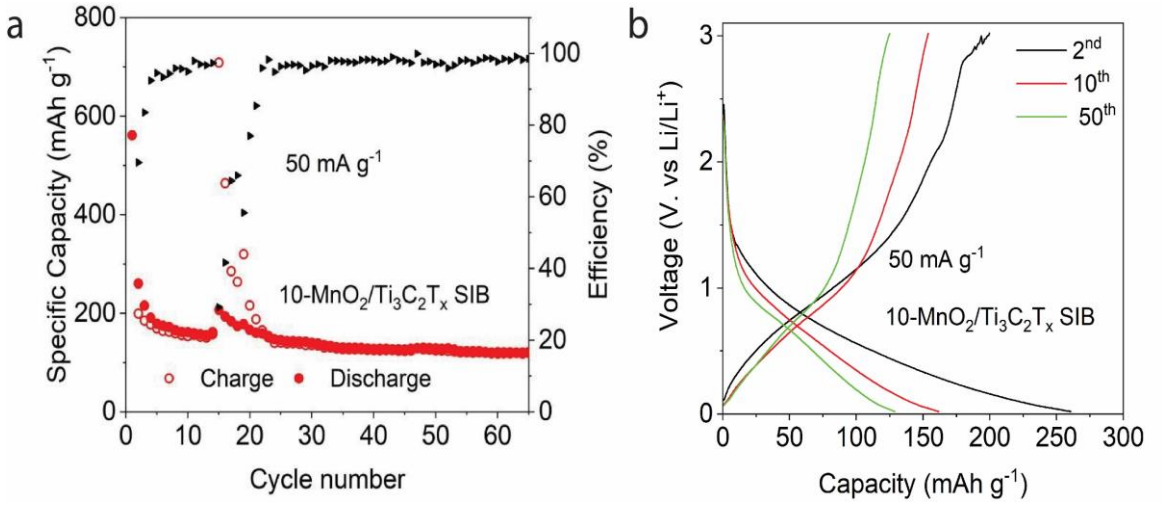

Fig.2.24 Electrochemical performance of 10-MnO_2/ $Ti_3C_2T_x$ as SIB anode at 50 mA g^{-1} :(a) cycling performance ;(b) galvanostatic charge/discharge profiles of 2^{nd}, 10^{th}, and 50^{th} cycles.

Chapter 3: Summary and conclusion

In this study, a stable and high specific capacity hybrid material, $SnO_x/Ti_3C_2T_x$, is successfully synthesized through a microwave-assisted hydrothermal method in a few minutes and its performance was investigated as a lithium battery anode material. From the structural characterization results through TEM, SEM and XRD, we were able to confirm the synthesis of a hybrid $SnO_x/Ti_3C_2T_x$ material. In the electrochemical test results, two factors affecting the material's capacity were studied; reaction time and $SnCl_2$: $Ti_3C_2T_x$ weight ratio. Based on the results, we concluded that the 5 min reaction time synthesized 10-$SnO_x/Ti_3C_2T_x$ is the best sample to work as a LIB's anode. In the half-cell test, the 5min 10-$SnO_x/Ti_3C_2T_x$ can perform with stable charging/discharging under 500 mA g^{-1} for more than 500 cycles and still has 583.7 mAh g^{-1} in long-term cycling performance, which shows its good electrochemical properties on specific capacity value and retention. Its high specific capacity is maintained even in higher current densities, which gives 430.4 mAh g^{-1} specific capacity at 2A g^{-1}. This result is better than traditional hydrothermal method synthesized Sn-carbon based anode for lithium-ion battery and has a much shorter experiment time. It is worth noting the specific capacity rising at high cycle numbers happens in the composite material as a result of $Ti_3C_2T_x$ lithium storage ability increasing with lithium-ion intercalation and deintercalation. This phenomenon proves the advantage of MXene as 2D material works together on LIB's anode since it inherits the advantage of both the TMO and MXene. This experiment exhibits a relatively simple process to produce different types of LIB anodes, and it can be useful to further related research. This method can also work for other types of TMO like MnO_2 or MoO_3 deposited on $Ti_3C_2T_x$ nanosheet, which proves it is a possible method to synthesis electrode materials in a short time.

Reference

1. Larcher, D. & Tarascon, J. M. Towards greener and more sustainable batteries for electrical energy storage. *Nat. Chem.* **7**, 19–29 (2015).
2. Chu, S., Cui, Y. & Liu, N. The path towards sustainable energy. *Nat. Mater.* **16**, 16–22 (2016).
3. Anasori, B., Lukatskaya, M. R. & Gogotsi, Y. 2D metal carbides and nitrides (MXenes) for energy storage. *Nat. Rev. Mater.* **2**, 16098 (2017).
4. Naguib, M., Mochalin, V. N., Barsoum, M. W. & Gogotsi, Y. 25th anniversary article: MXenes: A new family of two-dimensional materials. *Adv. Mater.* **26**, 992–1005 (2014).
5. Scrosati, B. & Garche, J. Lithium batteries: Status, prospects and future. *J. Power Sources* **195**, 2419–2430 (2010).
6. Zhang, X., Hou, L., Ciesielski, A. & Samorì, P. 2D Materials Beyond Graphene for High-Performance Energy Storage Applications. *Adv. Energy Mater.* **6**, (2016).
7. Choi, J. W. & Aurbach, D. Promise and reality of post-lithium-ion batteries with high energy densities. *Nat. Rev. Mater.* **1**, (2016).
8. Li, L. *et al.* Electrospun porous SnO2nanotubes as high capacity anode materials for lithium ion batteries. *Electrochem. commun.* **12**, 1383–1386 (2010).
9. Mei, J., Liao, T. & Sun, Z. Two-dimensional metal oxide nanosheets for rechargeable batteries. *J. Energy Chem.* **27**, 117–127 (2018).
10. Zhao, M. Q. *et al.* 2D titanium carbide and transition metal oxides hybrid electrodes for Li-ion storage. *Nano Energy* **30**, 603–613 (2016).
11. Nitta, N., Wu, F., Lee, J. T. & Yushin, G. Li-ion battery materials: Present and future. *Mater. Today* **18**, 252–264 (2015).
12. Ke, Q. & Wang, J. Graphene-based materials for supercapacitor electrodes – A review. *J. Mater.* **2**, 37–54 (2016).
13. Conway, B. E. Transition from “Supercapacitor” to “Battery” Behavior in

Electrochemical Energy Storage. *J. Electrochem. Soc.* **138**, 1539 (1991).

14. Fu, K. *et al.* Graphene Oxide-Based Electrode Inks for 3D-Printed Lithium-Ion Batteries. *Adv. Mater.* **28**, 2587–2594 (2016).
15. Hu, Y., Wu, Y. & Wang, J. Manganese-Oxide-Based Electrode Materials for Energy Storage Applications: How Close Are We to the Theoretical Capacitance? *Adv. Mater.* **1802569**, 1802569 (2018).
16. Liu, C., Yu, Z., Neff, D., Zhamu, A. & Jang, B. Z. Graphene-based supercapacitor with an ultrahigh energy density. *Nano Lett.* **10**, 4863–4868 (2010).
17. Peng, L., Fang, Z., Zhu, Y., Yan, C. & Yu, G. Holey 2D Nanomaterials for Electrochemical Energy Storage. *Adv. Energy Mater.* **8**, 1–19 (2018).
18. Naguib, M. *et al.* Two-dimensional nanocrystals produced by exfoliation of Ti3AlC2. *Adv. Mater.* **23**, 4248–4253 (2011).
19. Sun, Y., Chen, D. & Liang, Z. Two-dimensional MXenes for energy storage and conversion applications. *Mater. Today Energy* **5**, 22–36 (2017).
20. Hong Ng, V. M. *et al.* Recent progress in layered transition metal carbides and/or nitrides (MXenes) and their composites: synthesis and applications. *J. Mater. Chem. A* **5**, 3039–3068 (2017).
21. Ghidiu, M., Lukatskaya, M. R., Zhao, M., Gogotsi, Y. & Barsoum, M. W. Conductive two-dimensional titanium carbide 'clay' with high volumetric capacitance. *Nature* **516**, 78–81 (2014).
22. Xie, Y. *et al.* Role of Surface Structure on Li-Ion Energy Storage Capacity of Two-Dimensional Transition-Metal Carbides. (2014). doi:10.1021/ja501520b
23. Naguib, M. *et al.* MXene: A promising transition metal carbide anode for lithium-ion batteries. *Electrochem. commun.* **16**, 61–64 (2012).
24. Tang, Q., Zhou, Z. & Shen, P. Are MXenes promising anode materials for Li ion batteries? Computational studies on electronic properties and Li storage capability of Ti3C2 and Ti3C2X2 (X = F, OH) monolayer. *J Am Chem Soc* **134**, 16909–16916 (2012).
25. VahidMohammadi, A. *et al.* Thick and Freestanding MXene/PANI Pseudocapacitive

Electrodes with Ultrahigh Specific Capacitance. *J. Mater. Chem. A* (2018). doi:10.1039/C8TA05807E

26. Yan, J. *et al.* Flexible MXene/Graphene Films for Ultrafast Supercapacitors with Outstanding Volumetric Capacitance. *Adv. Funct. Mater.* **27**, 1–10 (2017).
27. Niu, S. *et al.* MXene-Based Electrode with Enhanced Pseudocapacitance and Volumetric Capacity for Power-Type and Ultra-Long Life Lithium Storage. *ACS Nano* **12**, 3928–3937 (2018).
28. Dong, Y. *et al.* All-MXene-Based Integrated Electrode Constructed by Ti3C2Nanoribbon Framework Host and Nanosheet Interlayer for High-Energy-Density Li-S Batteries. *ACS Nano* **12**, 2381–2388 (2018).
29. Vahidmohammadi, A., Hadjikhani, A., Shahbazmohamadi, S. & Beidaghi, M. Two-Dimensional Vanadium Carbide (MXene) as a High-Capacity Cathode Material for Rechargeable Aluminum Batteries. *ACS Nano* **11**, 11135–11144 (2017).
30. VahidMohammadi, A., Mojtabavi, M., Caffrey, N. M., Wanunu, M. & Beidaghi, M. Assembling 2D MXenes into Highly Stable Pseudocapacitive Electrodes with High Power and Energy Densities. *Adv. Mater.* **31**, 1–9 (2019).
31. Liu, Y. T. *et al.* Self-Assembly of Transition Metal Oxide Nanostructures on MXene Nanosheets for Fast and Stable Lithium Storage. *Adv. Mater.* **30**, 1–9 (2018).
32. Reddy, M. V., Subba Rao, G. V. & Chowdari, B. V. R. Metal Oxides and Oxysalts as Anode Materials for Li Ion Batteries. *Chem. Rev.* **113**, 5364–5457 (2013).
33. Jiang, J. *et al.* Recent advances in metal oxide-based electrode architecture design for electrochemical energy storage. *Adv. Mater.* **24**, 5166–5180 (2012).
34. Design, N. C., Society, M., Computer, T. & Society, A. M. Nano-sizedtransition-metaloxidesas negative-electrode materials for lithium-ion batteries P. *Nature* **407**, (2000).
35. Thackeray, M. M., Wolverton, C. & Isaacs, E. D. Electrical energy storage for transportation - Approaching the limits of, and going beyond, lithium-ion batteries. *Energy Environ. Sci.* **5**, 7854–7863 (2012).
36. Li, L., Raji, A. R. O. & Tour, J. M. Graphene-wrapped MnO2-graphene nanoribbons as

anode materials for high-performance lithium ion batteries. *Adv. Mater.* **25**, 6298–6302 (2013).

37. Kim, H. S. *et al.* Oxygen vacancies enhance pseudocapacitive charge storage properties of MoO3-x. *Nat. Mater.* **16**, 454–462 (2017).
38. Huang, R. *et al.* Irradiated Graphene Loaded with SnO2Quantum Dots for Energy Storage. *ACS Nano* **9**, 11351–11361 (2015).
39. Zhou, X., Wan, L. J. & Guo, Y. G. Binding SnO2 nanocrystals in nitrogen-doped graphene sheets as anode materials for lithium-ion batteries. *Adv. Mater.* **25**, 2152–2157 (2013).
40. Park, M. S. *et al.* Preparation and electrochemical properties of SnO2 nanowires for application in lithium-ion batteries. *Angew. Chemie - Int. Ed.* **46**, 750–753 (2007).
41. Wang, J. *et al.* Three-Dimensional Graphene/Single-Walled Carbon Nanotube Aerogel Anchored with SnO_2 Nanoparticles for High Performance Lithium Storage. *ACS Appl. Mater. Interfaces* **9**, 3544–3553 (2017).
42. Kayali, E., Vahidmohammadi, A., Orangi, J. & Beidaghi, M. Controlling the Dimensions of 2D MXenes for Ultrahigh-Rate Pseudocapacitive Energy Storage. *ACS Appl. Mater. Interfaces* **10**, 25949–25954 (2018).
43. Electrodes, L. M. Thin-Film Crystalline SnO2-Lithium Electrodes. *Society* **145**, 373–378 (1998).
44. Xiong, J. *et al.* Synergistically enhanced lithium storage performance based on titanium carbide nanosheets (MXene) backbone and SnO2quantum dots. *Electrochim. Acta* **268**, 503–511 (2018).
45. Lee, S. Y. *et al.* Unveiling origin of additional capacity of SnO2anode in lithium-ion batteries by realistic ex situ TEM analysis. *Nano Energy* **19**, 234–245 (2016).
46. Wang, S., Jiang, S. P. & Wang, X. Microwave-assisted one-pot synthesis of metal/metal oxide nanoparticles on graphene and their electrochemical applications. *Electrochim. Acta* **56**, 3338–3344 (2011).
47. Ahmed, B., Anjum, D. H., Gogotsi, Y. & Alshareef, H. N. Atomic layer deposition of

SnO2on MXene for Li-ion battery anodes. *Nano Energy* **34**, 249–256 (2017).

48. Sun, X. *et al.* Facile construction of ultrathin SnOx nanosheets decorated MXene (Ti3C2) nanocomposite towards Li-ion batteries as high performance anode materials. *Electrochim. Acta* **295**, 237–245 (2019).
49. Zhang, C. *et al.* Carbon-coated SnO2/graphene nanosheets as highly reversible anode materials for lithium ion batteries. *Carbon N. Y.* **50**, 1897–1903 (2012).
50. Zheng, W. *et al.* Microwave-assisted synthesis of three-dimensional MXene derived metal oxide/carbon nanotube/iron hybrids for enhanced lithium-ions storage. *J. Electroanal. Chem.* **835**, 205–211 (2019).